Long range acoustic imaging of the continental shelf environment: The Acoustic Clutter Reconnaissance Experiment 2001

Purnima Ratilal,[a),b)] Yisan Lai, Deanelle T. Symonds, and Lilimar A. Ruhlmann
Massachusetts Institute of Technology, Cambridge, Massachusetts 02139

John R. Preston
Applied Research Lab, Pennsylvania State University, State College, Pennsylvania 16804

Edward K. Scheer
Woods Hole Oceanographic Institute, Woods Hole, Massachusetts 02543

Michael T. Garr
Naval Undersea Warfare Center, Newport, Rhode Island 02841

Charles W. Holland
Saclant Undersea Research Center, San Bartolomeo, La Spezia, Italy

John A. Goff
University of Texas Institute for Geophysics, Austin, Texas 78759

Nicholas C. Makris
Massachusetts Institute of Technology, Cambridge, Massachusetts 02139

An active sonar system is used to image wide areas of the continental shelf environment by long-range echo sounding at low frequency. The bistatic system, deployed in the STRATAFORM area south of Long Island in April–May of 2001, imaged a large number of prominent clutter events over ranges spanning tens of kilometers in near real time. Roughly 3000 waveforms were transmitted into the water column. Wide-area acoustic images of the ocean environment were generated in near real time for each transmission. Between roughly 10 to more than 100 discrete and localized scatterers were registered for each image. This amounts to a total of at least 30 000 scattering events that could be confused with those from submerged vehicles over the period of the experiment. Bathymetric relief in the STRATAFORM area is extremely benign, with slopes typically less than 0.5° according to high resolution (30 m sampled) bathymetric data. Most of the clutter occurs in regions where the bathymetry is locally level and does not coregister with seafloor features. No statistically significant difference is found in the frequency of occurrence per unit area of repeatable clutter inside versus outside of areas occupied by subsurface river channels. © *2005 Acoustical Society of America.* [DOI: 10.1121/1.1799252]

I. INTRODUCTION

A long-range bistatic sonar system was used to rapidly image wide areas of the New Jersey continental shelf environment south of Long Island in a field experiment from 27 April to 5 May 2001.[1] The system consisted of a horizontally towed receiving array and two low-frequency vertical source arrays. Source signals were transmitted over long ranges to image scatterers up to tens of kilometers away. Waveguide scattering[2–6] and propagation[7] determine the performance of this remote sensing technology.

The field experiment, known as the 2001 Acoustic Clutter Reconnaissance Experiment (ACRE),[1] is a part of the U.S. Office of Naval Research Shallow Water Acoustic Clutter Program. The main objectives of the Program are to (1) determine the spatial and temporal variability of clutter in long range active sonar in continental shelf environments with generally low bathymetric relief, (2) identify the dominant sources of clutter, (3) understand the physical mechanisms that lead to these prominent returns, and (4) analyze the bistatic scattering characteristics of these dominant sources. In this context, clutter refers to scattering from objects in the environment that stand prominently above the diffuse and temporally decaying reverberation background that can camouflage or be confused with the returns from an intended target.

Another purpose of ACRE was to test the possibility of using low-frequency active sonar systems to rapidly image subseafloor geomorphology over wide areas in shallow water. In deep water, several remote sensing experiments have consistently and repeatedly observed strong and deterministic clutter return from lineated ridges and scarps on seamounts.[8–11] It was found that the level of the clutter is

---

[a)] Now at Northeastern University, Boston.
[b)] Electronic mail: purnima@ece.neu.edu

Report Documentation Page		*Form Approved* *OMB No. 0704-0188*

Public reporting burden for the collection of information is estimated to average 1 hour per response, including the time for reviewing instructions, searching existing data sources, gathering and maintaining the data needed, and completing and reviewing the collection of information. Send comments regarding this burden estimate or any other aspect of this collection of information, including suggestions for reducing this burden, to Washington Headquarters Services, Directorate for Information Operations and Reports, 1215 Jefferson Davis Highway, Suite 1204, Arlington VA 22202-4302. Respondents should be aware that notwithstanding any other provision of law, no person shall be subject to a penalty for failing to comply with a collection of information if it does not display a currently valid OMB control number.

1. REPORT DATE **APR 2005**	2. REPORT TYPE	3. DATES COVERED **00-00-2005 to 00-00-2005**
4. TITLE AND SUBTITLE **Long Range Acoustic Imaging of the Continental Shelf Environment: The Acoustic Clutter Reconnaissance Experiment 2001**		5a. CONTRACT NUMBER
		5b. GRANT NUMBER
		5c. PROGRAM ELEMENT NUMBER
6. AUTHOR(S)		5d. PROJECT NUMBER
		5e. TASK NUMBER
		5f. WORK UNIT NUMBER
7. PERFORMING ORGANIZATION NAME(S) AND ADDRESS(ES) **Massachusetts Institute of Technology,Cambridge,MA,02139**		8. PERFORMING ORGANIZATION REPORT NUMBER
9. SPONSORING/MONITORING AGENCY NAME(S) AND ADDRESS(ES)		10. SPONSOR/MONITOR'S ACRONYM(S)
		11. SPONSOR/MONITOR'S REPORT NUMBER(S)
12. DISTRIBUTION/AVAILABILITY STATEMENT **Approved for public release; distribution unlimited**		
13. SUPPLEMENTARY NOTES		
14. ABSTRACT		
15. SUBJECT TERMS		

16. SECURITY CLASSIFICATION OF:			17. LIMITATION OF ABSTRACT	18. NUMBER OF PAGES	19a. NAME OF RESPONSIBLE PERSON
a. REPORT **unclassified**	b. ABSTRACT **unclassified**	c. THIS PAGE **unclassified**	**Same as Report (SAR)**	**22**	

Standard Form 298 (Rev. 8-98)
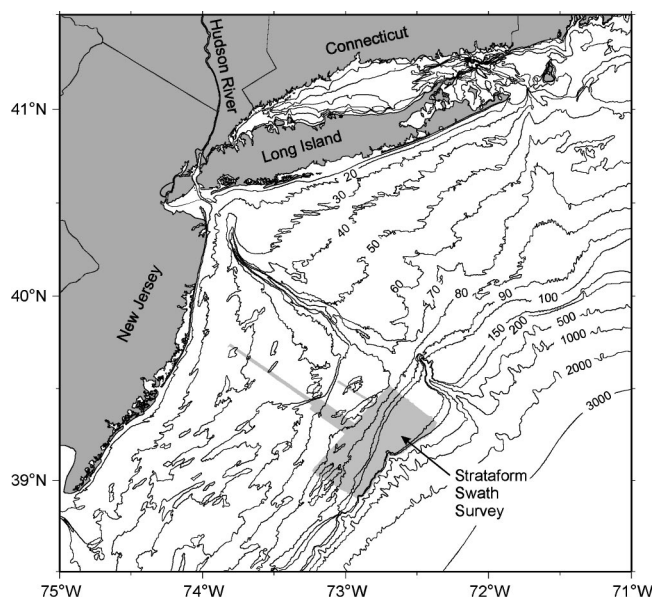Prescribed by ANSI Std Z39-18

FIG. 1. Location of the East Coast STRATAFORM area off the New Jersey coast. Contours in meters.

proportional to the projected area of the scarp along the path from target to bistatic source and receiver.[8–10] Attempting to draw an analogy with the deep water results, a number of investigators, for example in Ref. 12, proposed subseafloor geomorphology, which exists throughout the continental shelf, to be potential source for anomalous sonar returns in areas of level bathymetry in shallow water.

The New Jersey STRATAFORM[13] site, shown in Fig. 1, was well-suited for ACRE because a number of substantial geophysical surveys[14–16] have previously characterized seafloor and subbottom features over wide areas. Furthermore, several other acoustic experiments have been conducted in this area to investigate acoustic propagation conditions[17] and to invert for seabottom properties.[18,19] Data from the geophysical surveys are used here to identify natural features of the seafloor and subseafloor that might possibly be imaged by our remote acoustic sensing system.

During the ACRE, two research vessels were used to acquire both monostatic and bistatic scattering data. Roughly 3000 waveforms were transmitted into the water column from vertical source arrays in the 390- to 440-Hz band and received by a horizontal towed array. A wide-area acoustic intensity map (image) of the environment was generated for each transmission. On average from 10 to 100 discrete and localized scattering events were registered per transmission. From a clutter perspective, this gives a total of at least 30 000 scattering events that could be confused with that from a large submerged vehicle over the period of the experiment. Two acoustic targets,[1,20] essentially cylindrical air-filled elastic tubes approximately 30 m long, with known scattering properties and locations were vertically deployed and used to calibrate returns and confirm theories about waveguide scattering from extended objects and long-range imaging in continental shelf environments.

In this paper, wide-area acoustic images from the ACRE are presented to illustrate the prominent and discrete scattering events measured in the New Jersey continental shelf en-

vironment. Returns that coincide with the location of the calibrated targets are evident in the images indicating our ability to accurately chart the returns in both space and time. Most of the charted clutter were found to occur in regions where the bathymetry is locally level and do not coregister with any known geologic features of the seafloor. Some of the charted clutter appears to occasionally correspond with buried river channels identified from geophysical surveys. However, statistical analysis of the clutter in regions where the subbottom geomorphology has been mapped shows that there is no significant difference between the frequency of occurrence per unit area of repeatable clutter events that chart within areas occupied by buried river channels and those that chart outside of areas occupied by channels.

In Sec. II, we provide a description of the New Jersey STRATAFORM area geology and a detailed description of the ACRE. In Sec. III, we explain how long-range acoustic data are processed to generate wide-area images. Images showing the charted clutter and returns from the calibrated targets are presented in Sec. IV. Possible mechanisms for the clutter returns are discussed in Sec. V. Oceanographic data collected during the experiment, such as sound speed structure, are presented in the appendix.

II. DESIGN AND IMPLEMENTATION OF THE ACRE

Prior to the ACRE, a number of geophysical surveys[14–16] at the New Jersey STRATAFORM site characterized the seafloor and subbottom features over wide areas. Figure 2 shows the water depth at the STRATAFORM site where bathymetric data are available at 30 m horizontal resolution.[15] Seabed and subbottom features identified from the geophysical surveys are overlain on the bathymetry. The candidate features for prominent scattering include incised or buried river channels, relict iceberg scours and surface erosional features on the seafloor, and surface or near surface outcroppings of seismically reflective subsurface strata within the seabed. Figure 3 shows an interpretation of a seismic profile from Ref. 14 of several river channels buried at different depths from the seafloor intersecting with various sub-bottom strata. Apart from these geologic features, aggregates of compact scatterers such as gravel deposits on the seafloor, gas pockets in the seabed, and large and densely populated schools of fish are also possible sources of clutter.

Figure 4 shows the directional derivative (DD) of bathymetry at the STRATAFORM area. The DD is defined in Ref. 21 as the dot product of the gradient of bathymetry with the horizontal unit vector pointing in the direction of an observation point. In Fig. 4, the DD is plotted for an observation point to the north of the STRATAFORM area. Seafloor surfaces facing the observation point have positive DD, surfaces facing away have negative DD, and level surfaces have zero DD. Inspection of Fig. 4 shows that the experiment site has mostly benign slopes of less than 0.5° with few discrete features on the seafloor. Even the seafloor features that are noticeable, such as the iceberg scours and erosion pits, have small slopes typically <3°. Their vertical relief is typically smaller than the acoustic wavelength of roughly 4 m in this experiment.

Ratital et al.: Acoustic clutter reconnaissance experiment 2001

In both Figs. 2 and 4, the subbottom features shown are based on interpretations of geophysical data acquired *prior* to the ACRE 2001. The areas where the subsurface features are shown are the only areas where the subbottom data had been acquired and analyzed prior to the ACRE 2001. There may be other subsurface features elsewhere in the figure, but the geophysical data had either not been collected in those areas or had not been analyzed prior to the experiment. The most current geophysical interpretations of the subsurface features is provided and used in our analysis of the measured clutter in Sec. IV.

The experiment was conducted using the Research Vessel (RV) *Endeavor* and the NATO Research Vessel (NRV) *Alliance* (Fig. 5). RV *Endeavor* was used mainly as a source ship for bistatic measurements. It deployed a source system used by the Multistatic ASW Capability Enhancement Program (MACE) consisting of a seven-element array of uniformly spaced XF-4 transducers, beamed to transmit at broadside during the whole experiment. RV *Endeavor* was fastened to moorings at three sites where a fixed transmission location was maintained for the bistatic measurements. NRV *Alliance* was the only ship that deployed a horizontal receiving array. It also deployed a two-element MOD40 transducer source system that was towed for quasi-monostatic measurements. A nominal tow speed of 2 m/s was maintained throughout the measurements by NRV *Alliance*. The horizontal receiving array was a 256-element line array with three nested apertures, each consisting of 128 sensor elements evenly spaced at 0.5, 1, or 2 m, respectively. Only data from 128 elements at 1-m spacing are analyzed in this paper. For a sound speed of 1500 m/s, this subaperture corresponds to an array cut for 750 Hz. Each of the two calibrated targets,[1,20] deployed at a selected site, were moored to the bottom in waters approximately 80 m deep, 18 m off the seafloor. They stood vertically in the water column spanning roughly 32- to 62-m depth from their own buoyancy.

The tracks traversed by NRV *Alliance*, mooring locations of RV *Endeavor*, and locations of the two calibrated targets and subbottom features are also plotted in Fig. 4. Acoustic transmissions were centered about three distinct sites of the STRATAFORM area identified as sites 1, 2, and 3. The water depth at the three sites ranged from approximately 70 to 130 m. At site 1, the tracks of NRV *Alliance* and the source location for RV *Endeavor* were designed to image the buried river channels and shallow subsurface reflectors truncated at the seafloor.[14,15] At site 2, the erosion pits on the seafloor and the subsurface reflectors, as well as the calibrated targets, were the focus of the measurement. The tracks at site 3 were designed to image the iceberg scours and more subsurface reflectors and to obtain scattered returns from the Hudson Canyon walls. The large number of tracks at each site was neccessary to study the range and azimuth dependence of the scattering and to distinguish returns from the various candidate clutter targets at a variety of ranges and azimuths. The numerous tracks also served to help break the ambiguity inherent in line array measurements.

The sources transmitted both linear frequency modulated (LFM) and sinusoids or "continous wave" (CW) signals of varying duration in the frequency range from 390 to 440 Hz.[1] For the bistatic transmissions by RV *Endeavor*, the LFM signals were shaded with a Tukey window while the CW signals were shaded with a Hann window. For the quasi-monostatic transmissions by RV *Alliance*, a rectangular window was used in all transmissions for both the LFM and CW signals. The length of each NRV *Alliance* track line is roughly 10 km and the waveforms were transmitted at every 50- or 100-s interval. With a speed of 2 m/s for the receiver ship, data from a total of roughly 50 or 100 transmissions were measured along each track.

III. WIDE-AREA IMAGES OF THE OCEAN ENVIRONMENT

A. Generating images in near-real-time

During the ACRE, a wide-area image of received sound pressure level as a function of horizontal position over tens of kilometers was generated for every transmission (ping) in near-real-time. For a given transmission, two-way travel time was used to determine the range of returns and beamforming to determine the azimuth. The process has been previously described in Refs. 8, 21, and 11. It follows the same principles used in high-frequency side-scan sonar, medical ultrasound, and radar image processing except that the present imaging process involves the complexities of multipath propagation, waveguide scattering, and dispersion.

In this paper, echo returns from mono- and bistatic LFM transmissions of varying duration measured with NRV *Alliance*'s horizontal line array with 128 elements at 1-m spacing are analyzed. The raw time series data for each hydrophone were filtered, demodulated, and decimated. This decimated array data were then converted to beam-time data by time-domain beamforming. The sharpest cross-range resolution is at broadside, where the signals arrive almost perpendicular to the array axis. The broadest cross-range resolution is near endfire, where the signals arrive almost parallel to the array axis.

A Hanning spatial window function was applied in the beamforming to reduce sidelobe levels where the first sidelobe level is down 30 dB from the main lobe. This was important for reducing sidelobe leakage from radiated noise present in beams containing the source ship which was moored near the features to be imaged. Following Eqs. (1) and (2) of Ref. 21, the 3-dB beamwidth β of the array is approximated using

$$\beta(\varphi) \approx 1.3 \frac{\lambda}{L \cos \varphi}, \tag{1}$$

for steering angles from broadside $\varphi = 0$ to a transition angle φ_t near endfire, $\varphi = \pi/2$, where λ is the wavelength and L is the array length. As φ approaches φ_t, ambiguous beamwidths each reach a value approximately equal to that at endfire, and begin to merge until they completely overlap at endfire where the beamwidth is

$$\beta(\varphi = \pi/2) \approx 2.8 \sqrt{\lambda/L}. \tag{2}$$

For the array aperture of 127 m, the optimal 3-dB resolution is about 2.1° at broadside and 27° at endfire. This corresponds to a cross-range resolution $\Delta \rho = \rho \beta$ of 364 m at
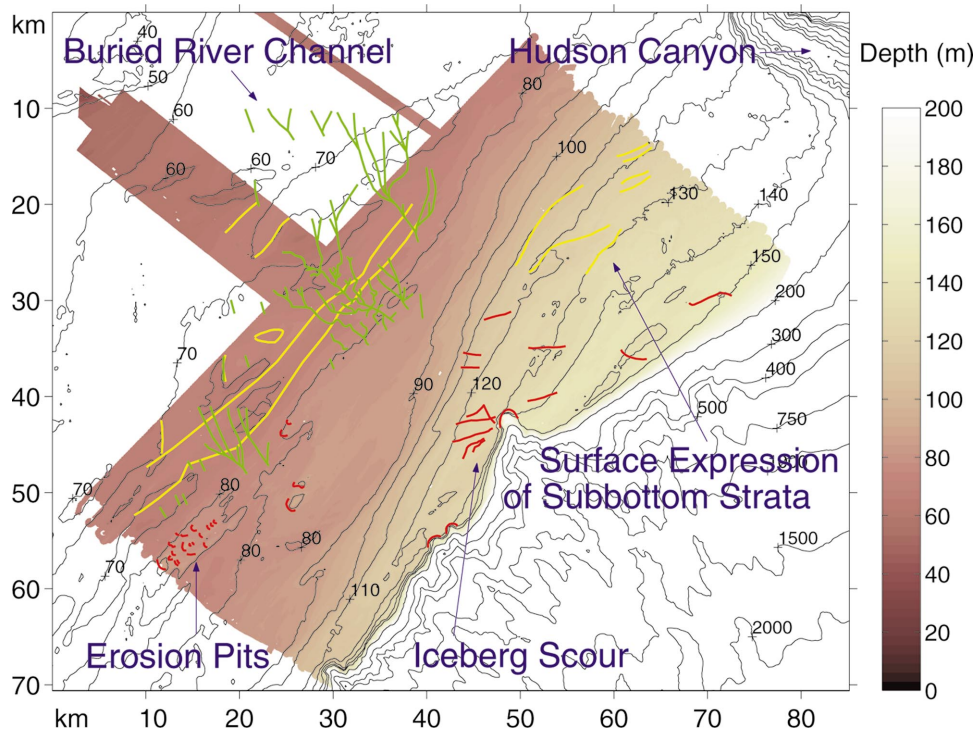
FIG. 2. Bathymetry of the STRATAFORM area with shaded region sampled at 30-m interval. Candidate features identified from previous geophysical surveys[14,15] that might give prominent and coherent scattered returns include incised or buried river channels (green), relict iceberg scours and erosion pits on the seafloor (red), and surface or near-surface expression of seismically reflective subsurface strata within the seabed (yellow). Coordinates of x and y axis origin in the north-west corner: 39° 31.00′N, 73° 17.28′W.
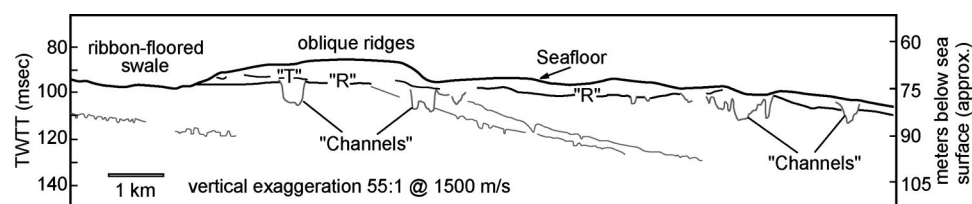
FIG. 3. Interpreted seismic line, adapted from Ref. 14, showing the shallow stratigraphy within site 1. The figure shows numerous buried river channels intersected by highly reflective subbottom strata. One of these subbottom strata is called an R-reflector.
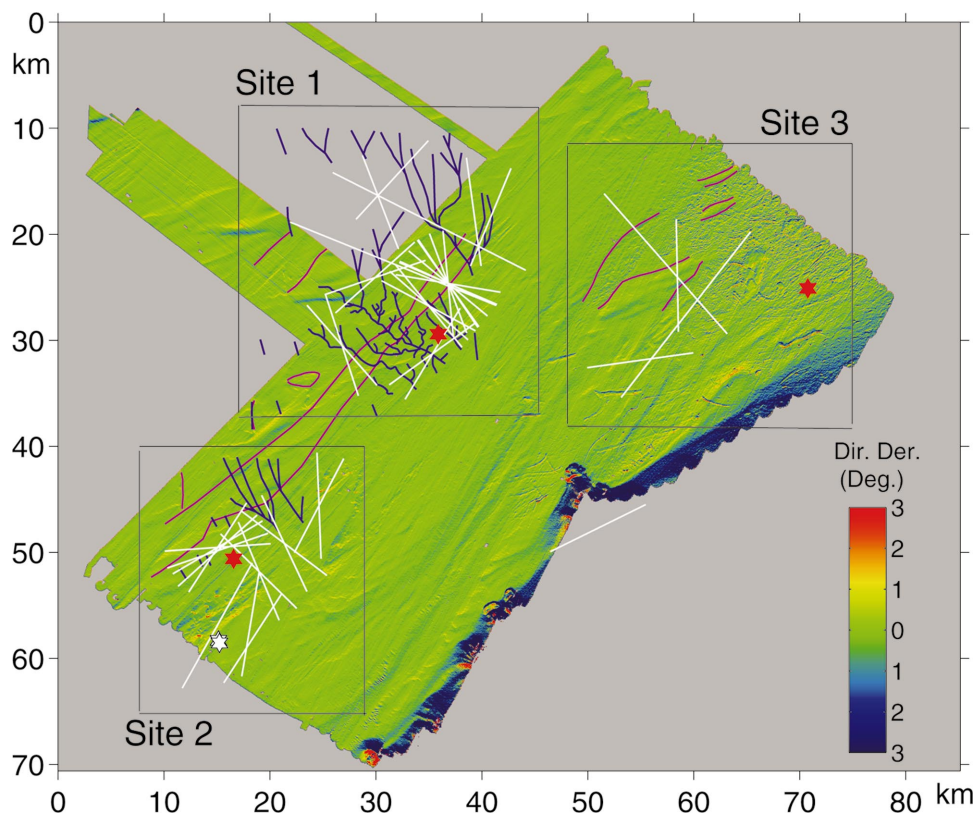

FIG. 4. Directional derivative of the 30-m sampled bathymetry at the STRATAFORM site with respect to a source far in the north. The seafloor is mostly level locally with slopes of <1/2°. There are very few discrete features such as iceberg scours and erosion pits on the seafloor with slopes of at most 3°. Acoustic transmissions were centered about three distinct sites in the STRATAFORM area. Overlain are the tracks traversed by NRV *Alliance* (white lines), mooring locations of RV *Endeavor* (red stars), location of the two calibrated targets (white stars), and subbottom features (blue and pink lines). Coordinates of x and y axis origin in the north-west corner: 39° 31.00′N, 73° 17.28′W.
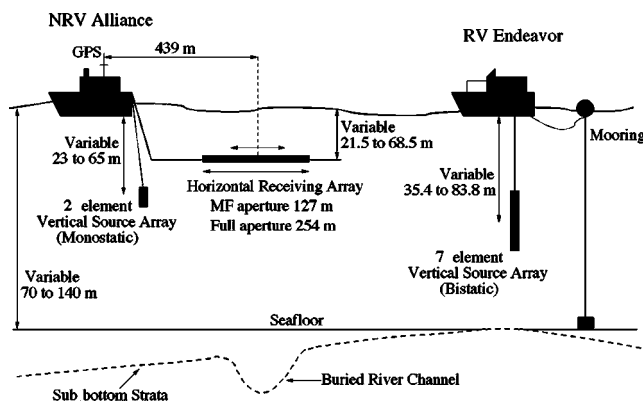
FIG. 5. A sketch of NRV *Alliance* towing a two-element vertical source array at 1.875-m spacing and a 256-element horizontal receiving array with spacing between elements of 0.5, 1, and 2 m. Only data from 128 elements of the receiving array at 1-m spacing are analyzed in this paper. The mean depth of the NRV *Alliance* two-element source was varied between 23 and 65 m. The mean depth of the receiver array was varied from 22 to 68 m. RV *Endeavor* was moored at each site where measurements were collected and it deployed the MACE source system consisting of a 7-element array spaced at 1.625 m. The mean depth of the MACE source was varied between 35 and 84 m and it was beamed to transmit at broadside throughout the experiment. The water depth at the three measurement sites ranged from approximately 70 to 130 m.

broadside and of 4.7 km at endfire at a range of $\rho = 10$ km, which is a typical range for detecting the clutter events during the experiment.

The beam-time data are linearly converted to beam-range data by multiplying the total two-way travel time with half the mean sound speed c which was taken to be 1475 m/s based on measured sound speed in the water column (see Appendix A). To improve on the range resolution and signal-to-additive-noise ratio, the LFM data from 390 to 440 Hz were match filtered with a replica of the source signal to give an effective range resolution of $c/2B \approx 15$ m, where the bandwidth B is 50 Hz. The data were then averaged to 30 m resolution and then mapped to a Cartesian grid with the same 30×30 m^2 grid increment as the high resolution bathymetry data used. The mapping procedure accounts for beam overlap by an incoherent averaging of adjacent beams.[22]

Multi-modal propagation in a shallow water waveguide leads to time spread and delay in the mean arrival time of signals. This dispersion effect is a result of the differing modes of the waveguide propagating the acoustic energy with varying group velocities, and is highly dependent upon the waveguide properties. It also varies as a function of range and depth due to modal interference which causes a change in the spatial and temporal structure of the signal. Simulations in various shallow water waveguides in Ref. 23 show that the error in charting returns from objects in the water column is about 200 m for the ranges relevant to this study after match filtering with the source signal. Charting error varies with the sound speed used to convert travel time to range. The charting error of 200 m is for a sound speed that corresponds to the minimum sound speed in the water column. This sound speed was found to provide the smallest errors in localizing a source or target in the water column.

During the experiment, fluctuations on the order of $\pm 3°$ were observed in the towed array heading sensor measure-

ments. At site 2, the GPS positioning of the calibrated targets relative to the source and receiver was used to provide a more accurate mean orientation of the receiver array for each track. The corrections needed for each track, however, were small, approximately 0° to 4°. Since no calibrated targets were present at sites 1 and 3, no corrections were applied to those images.

The standard deviation of a pixel value or an average of stationary pixel values in an acoustic image is now estimated.[8] We assume that the transmitted waveform's interaction with the seafloor scattering area completely randomizes the return such that the real and imaginary temporal components of the instantaneous scattered field are identically distributed and uncorrelated zero-mean Gaussian random variables. The instantaneous intensity of the return is then exponentially distributed and the time-averaged intensity is gamma distributed[24] with degrees of freedom μ corresponding to the time-bandwidth product TB of the scattered field,[25] where T is the measurement time. This product is an approximate measure of the number of independent and instantaneous intensity fluctuations averaged over T. If the reverberation level in dB *re* 1 μPa for a given pixel in the acoustic image is $R = 10 \log$ (mean square pressure), the standard deviation σ of the reverberation level in dB is[8,25]

$$\sigma(\mu) = 10(\log e) \sqrt{\zeta(2,\mu)}, \qquad (3)$$

where

$$\zeta(\nu,\mu) = \sum_{k=0}^{\infty} \frac{1}{(\mu+k)^{\nu}}, \quad \text{for} \quad \nu > 1, \quad \mu \neq 0, -1, -2, -3, ..., \qquad (4)$$

is the Riemann's zeta function. For an instantaneous intensity measurement, $\mu = 1$ and $\sigma(1) \approx 5.6$ dB. To reduce the standard deviation to 3 dB which is relatively negligible compared to the dynamic range of the levels spanned in the images produced in this experiment, an averaging time of $T = 0.04$ s is used. This corresponds to $\mu = 2.0$ for the $B = 50$ Hz bandwidth LFM transmissions analyzed in this paper. Stationary averaging of adjacent pixels would lead to a smaller standard deviation according to Eqs. (3) and (4), but will also reduce the spatial resolution. (We ignore averaging of overlapping beams because the measurements are not independent.) The prominent returns typically stand above the background reverberation by tens of decibels (many standard deviations) and are therefore considered to be deterministic.

B. Interpreting images generated with low frequency and long range towed array sonar

Figure 6 shows a wide-area image of the ocean environment at site 2 obtained from a single bistatic transmission with the receiver ship NRV *Alliance* oriented along track 17. The origin of the range axis along the x and y directions in the figure is at 39° 31.00′N, 73° 17.28′W. This origin is at the north-west corner of the images in Figs. 2 and 4. This fixed location for the range origin will be used for all acoustic intensity images presented in this paper. The array heading is measured with respect to true north increasing in a clockwise direction. The image shows both the diffuse back-
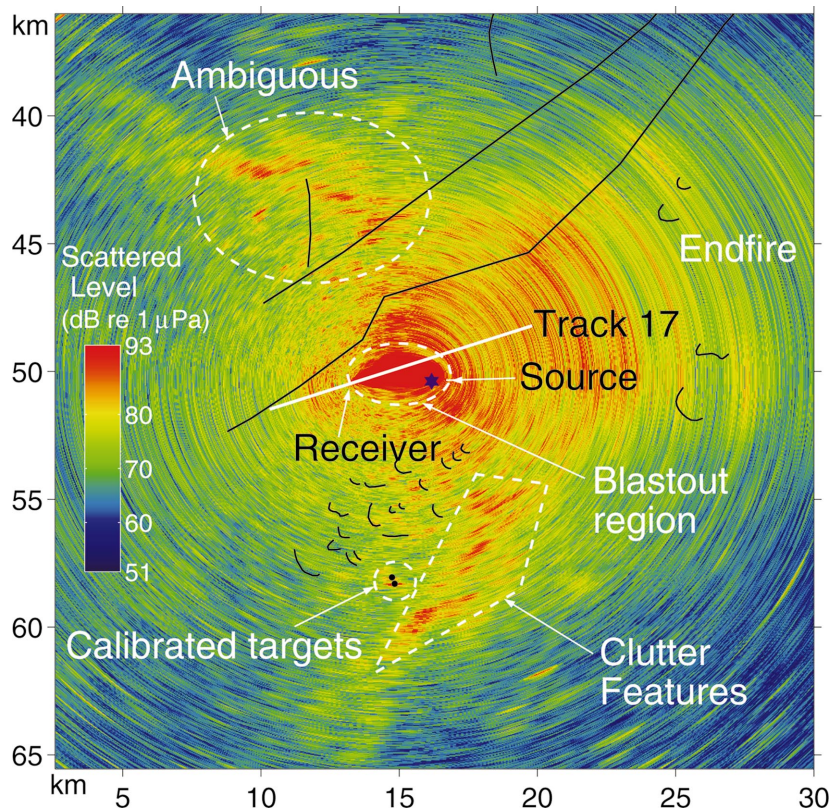
FIG. 6. A single-ping bistatic wide-area image along track 17 at site 2. Travel time to range conversions are done by multiplying the two-way travel time with half the mean sound speed of 1475 m/s. All returns are mirrored about the array axis (71° with respect to true north) due to left–right ambiguity. Two prominent and discrete scattering events >20 dB above the background co-register well with the location of the calibrated targets approximately 8.5 km to the south. Numerous other prominent scattering events (clutter features) that can be confused with returns from the calibrated targets are present in the image. Comparison with Fig. 8 breaks the receiver line array's left–right ambiguity and places the true location of these clutter features to the south within the dotted white trapezoid. (Date: 1 May, ping time: 13:04:30Z, transmission: 1-s duration LFM from 390 to 440 Hz, mean source depth: 55 m, mean receiver depth: 42 m, array heading: 71°.)
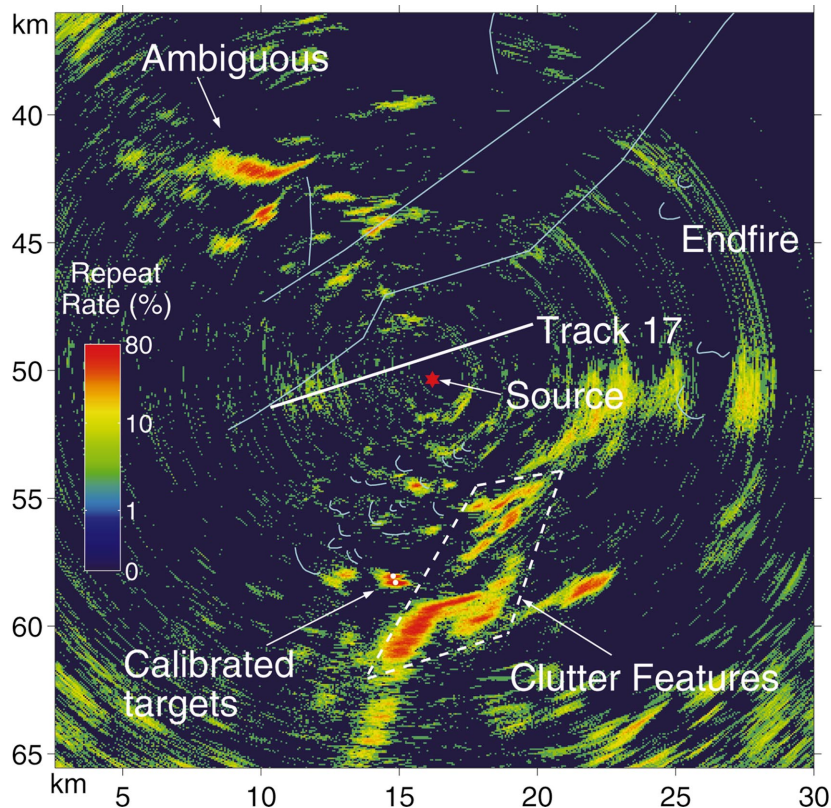

FIG. 7. Hotspot consistency chart from 49 bistatic LFM transmissions along track 17. The figure displays the number of images that register a strong scattering event >10 dB above the local average within 1.8×1.8 km^2 area of a given pixel location. Scattering events within the trapezoid as well as those from the calibrated targets are consistently prominent in most of the wide-area single ping images along track 17. Events within the trapezoid can either be confused with or camouflage those from the calibrated targets. (Date: 1 May, time: 12:37:00Z to 14:01:00Z, mean source depth: 55 m, mean receiver depth: 42 m, array heading: 71°.)

ground reverberation level in decibels from the ocean environment as well as strong scattered returns from the calibrated targets and other submerged objects or features. For each transmission, the signal first measured by the receiving array is that arriving directly from the source. This direct arrival is strong and gives rise to the blast-out region which appears as a red ellipse surrounding the source and the receiver in Fig. 6. The diffuse background reverberation scattered from random rough patches of the ocean environment, as well as the returns from the calibrated targets and other submerged objects or features arrive after the direct signal has passed. This environmental reverberation has a mean intensity that decays with range due to spreading and absorption loss in the waveguide. The rate of decay depends on the properties of the waveguide, such as the sound speed structure, attenuation in the water column and bottom, and surface and bottom inhomogeneities, as well as the measurement geometry. The decay in the reverberation provides vital information about the environment needed to model propagation and diffuse scattering. In Fig. 6, we do not average out the trend in the data since it would eliminate this vital information.

A horizontal line array has left–right ambiguity about the array axis that is expressed differently in monostatic and bistatic charts. Prominent returns are ambiguously charted nearly symmetrically about the receiving array axis in monostatic geometries. For bistatic geometry, ambiguity occurs on an ellipse with a major axis that passes through the source and receiver. A diagram illustrating the two-way travel time ellipse for bistatic measurements is provided in Ref. 9, where it is shown that distortion in the image may occur as the ambiguous returns are charted to either a smaller or broader spatial extent. The methods used in this paper to resolve the left–right ambiguity in the measurements are discussed further in Sec. III D. In Fig. 6, the left–right ambiguity is mapped onto ellipses at close ranges to the bistatic source and receiving array. At ranges larger than the source–receiver separation, the ambiguity about the array axis approaches circular symmetry.

During the ACRE, few monostatic measurements were made in comparison to the bistatic measurements because the monostatic source was weaker. As a result, we were not able to image very far out in range with the monostatic source. The rough maximum range before the acoustic imaging system became noise limited was on the order of 10 km for the monostatic source. For the bistatic source, this range was more than 50 km away from the source. Most of the images illustrated in this paper are from bistatic measurements.

C. Hotspot repeatability chart

In order to measure the frequency of occurrence of a strong scattering event from a target or feature along a given track, we generate a hotspot consistency chart for each track. First, a moving local peak detector is applied to a single wide-area image to detect pixels where the reverberation level stands more than 10 dB above the average for a 1.8 $\times 1.8$ km^2 subimage. These pixels are assigned a value of 1 and all others 0. Pixels in the blast-out region are assigned a

value of 0, since we are only interested in detecting targets and features in the environment. This binary matrix from each reverberation image is then summed for all the images along a track to form the hotspot consistency chart for each track. The hotspot repeatability chart for track 17 is shown in Fig. 7. A total of 49 bistatic acoustic images are combined to form this composite. In Fig. 7, a given pixel shows the number of images that register a strong scattering event >10 dB above the local average within 1.8×1.8 km^2 area of the pixel. The maximum of the legend in each hotspot repeatability chart is the maximum clutter repeatability in the given image.

The standard deviation[25] for the time-averaged diffuse reverberation is 3 dB as shown in Sec. III A. The local peak detector alogrithm thus picks out pixels with levels that are about three standard devations above the local mean within each subimage. Both scattered returns from fixed targets and diffuse background reverberation decay with range due to spreading and absorption loss. A globally fixed threshold detector is only useful if the decaying trend of the reverberation can be accurately removed before the detector is applied. It is usually difficult to detrend measured data accurately given the lack of *a priori* environmental information needed to model the trend. Our local peak detector takes the range decay into account empirically. It is also independent of the strength of the source, making it versatile and easy to implement.

We combine information contained in wide-area images acquired along a single track to form the hotspot consistency chart for the given track. This chart is found to be extremely useful in picking out strong and persistent echos as well as in resolving ambiguity in measurements along a single track as will be discussed in Secs. III D and IV. A hotspot consistency chart combining information from multiple track lines should be used with caution. Our attempts at combining data from all the tracks at a given site by forming an overall hotspot chart for the site were found to lead to confusion in identifying actual returns. This is because the many tracks at a given site have varying array headings and the same scatterers often do not appear on different tracks, making it impossible to resolve ambiguity by such a combination. Even when the same scatterers do appear on differing tracks the combination does not significantly reduce ambiguity but rather leads to multiple ambiguities that often mask true features as noted in Ref. 22.

D. Ambiguity resolution

Two methods are employed in the present analysis to resolve the left–right ambiguity in the returns from the horizontal line array. The first method involves comparing events from images obtained on tracks that have approximately similar location but where the array orientation differs.[8] In these tracks, the true returns will be consistently charted to the same location, while the ambiguous ones will be charted to different locations.

The second method resolves the ambiguity for measurements made along a single track with the use of the hotspot consistency chart for the track. This method is applicable in bistatic scenarios when the range to the feature is not much

larger than the source–receiver separation. It exploits the elliptical shape of the travel time locus to break the ambiguity in the line array measurement.

These two methods for ambiguity resolution will be pointed out in the images in Sec. IV.

IV. LONG RANGE ACOUSTIC IMAGING RESULTS

In this section we present the major experimental findings of the ACRE 2001. Roughly 3000 waveforms were transmitted into the water column and wide-area image of the reverberation from the ocean environment was generated in near-real-time for each transmission. From 10 to more than 100 discrete and localized clutter events (10 dB above the background) were registered for each image. This gives a total of at least 30 000 scattering events that could be confused with that from a large submerged vehicle over the period of the experiment. The vast majority of prominent and discrete scattering events appear in areas where the bathymetry is locally flat or with slopes less than 0.5°. This implies that these returns most probably do not originate from the seafloor and that they could be due to objects in the water column or possibly features in the subbottom.

In the following three subsections, individual ping and hotspot consistency images from various tracks at the three sites are shown. The clutter in these images is representative of the scattering events measured at each site. We begin our discussion with site 2 where the calibrated targets were deployed.

A. Site 2 with calibrated targets

In this section, we present wide-area images showing strong and discrete returns from the calibrated targets deployed in the waveguide at site 2. These images, which were acquired during the middle of the experiment, also show an organized pattern of prominent scattering events in a region of effectively flat bathymetry (slopes less than 0.5°), with water depths from 80 to 100 m, where the subbottom had not been well profiled. Subsequent geophysical surveys, specifically designed to explore the subbottom in the vicinity of these prominent scattering events at site 2, discovered a network of buried river channels.[26,27] Most of the prominent scattering events, however, did not coregister with the newly discovered river channels. The measurements at site 2 were repeated about 4 days later at the end of the experiment along tracks with nearly similar range and bistatic location for the track center, but with varying orientation. These measurements found the clutter events at site 2 to be highly variable across the tracks, all of which had differing headings. Since there was a 2-h time period for the data collection on each track, the clutter could also have evolved with time. A statistical analysis of the spatial distribution of repeatable clutter is given in Sec. IV A 2 to determine if the repeatable clutter favors any particular spatial location.

In Fig. 6, which shows a wide-area image from track 17 at site 2, we observe two prominent scattering events approximately 8.5 km away to the south of the source and receiving array that register well with the calibrated targets. These events stand out by more than 20 dB above the reverberation in surrounding areas. This difference is much larger than the received level standard deviation of 3 dB (shown in Sec. III A). The receiving line array has left–right ambiguity about the array axis. We therefore see the ambiguous returns from the calibrated targets charted to the west in Fig. 6.

We observe numerous other prominent and discrete scattering events in the image shown in Fig. 6. Many of these features are just as prominent as the calibrated targets, standing out by more than 20 dB above the reverberation in surrounding areas. These features can be confused with or camouflage the calibrated targets if the precise location of the targets are unknown.

To identify where the clutter originates, we break the receiving array's ambiguity by comparing Fig. 6 with Fig. 8, a bistatic transmission along track 14 which is at a similar range but slightly different orientation than track 17. In both Figs. 6 and 8, we observe consistently strong and prominent events within the trapezoid to the south of the source and receiving array. This shows that the region with the trapezoid is the true location of the clutter. The ambiguous events are charted to the west in both figures and are not in the same location. The differing array orientation in tracks 14 and 17 causes the false returns of the features to be charted to different regions.

To examine the repeatability of the prominent scattering events within the trapezoid as well as those from the calibrated targets, a hotspot consistency chart, as described in Sec. III C, is derived for track 17 and shown in Fig. 7. From Fig. 7, we observe that scattering events from the calibrated targets are repeatedly prominent as the receiver ship moves along the track. They appear as a local maxima in most of the 49 images along the track. The scattering events within the trapezoid in Fig. 7 are also prominent and repeatable. They appear in most of the charts with levels >10 dB above the local average.

In Fig. 9, we overlay the prominent events from Fig. 7 on the color directional derivative of bathymetry. Only events with levels that are 10 dB above the local average and are consistent in at least ten transmissions along the track are overlain. From Fig. 9, we infer that the prominent and consistent scattering events within the trapezoid do not originate from the seafloor surface because the seafloor in this region is level. The prominent events could have been caused by other objects submerged in the water column or features in the subbottom. Features in the subbottom may not be detectable using a conventional bathymetric depth-sounder, but can be found by subbottom profiling.

During the ACRE 2001, RV *Endeavor* explored the bottom with a hull-mounted chirp subbottom profiler in the vicinity of the prominent scattering events within the trapezoid in Figs. 6 and 7. More detailed geophysical surveys were carried out in this region using both deep-tow and hull-mounted subbottom profiling systems in August 2001[26,27] and May 2002 under the Acoustic Clutter Program. All three surveys found a network of buried river channels with flanks that shoal close to the seafloor in the vicinity of the scattering events. An interpretation[27] of the morphology of these buried river channels from the geologic data are shown in Fig. 10. Figure 11 shows a deep-tow chirp profile of several buried
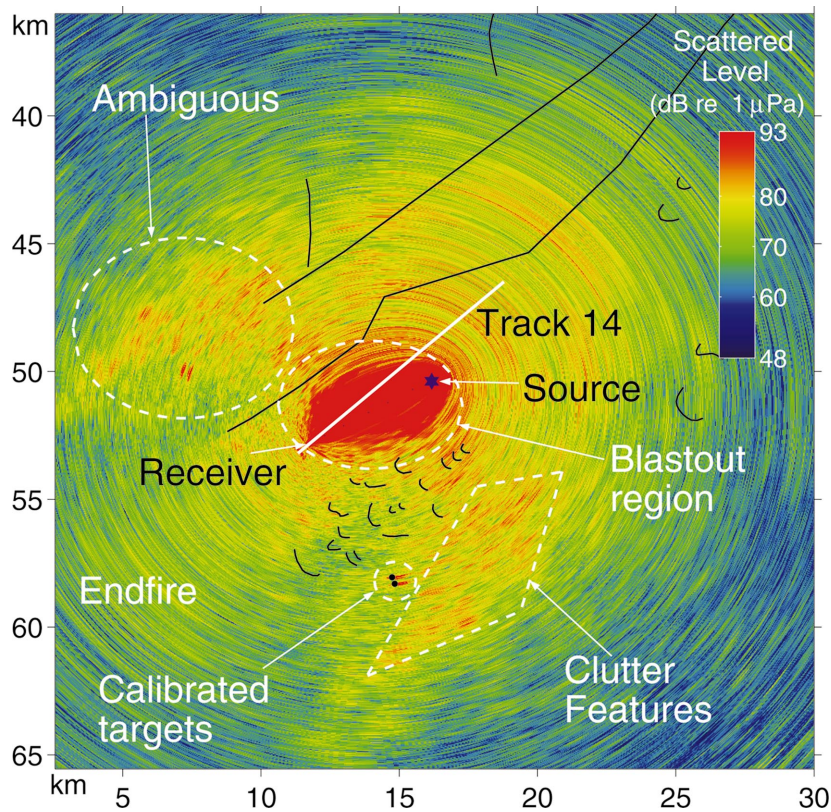
FIG. 8. Single-ping bistatic wide area image from track 14. Left–right ambiguity of the prominent scattering events from the features of interest can be resolved by comparing this figure with Fig. 6. (Date: 1 May, ping time: 11:35:00Z, transmission: 2-s duration LFM from 390 to 440 Hz, mean source depth: 55 m, mean receiver depth: 22 m, array heading: 226°.)
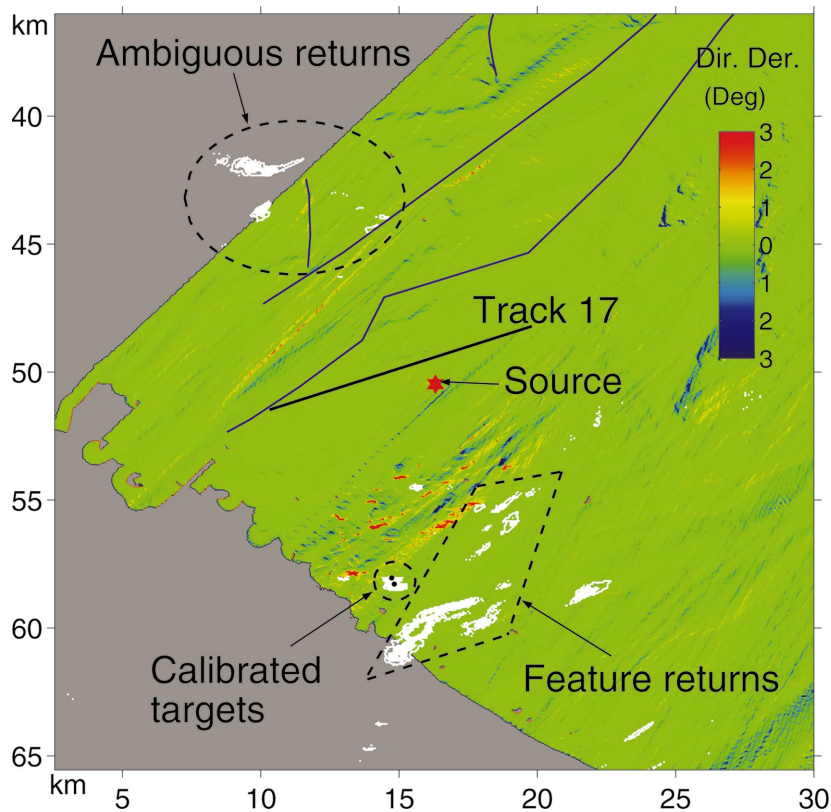

FIG. 9. Prominent events from the LFM transmissions on track 17, as shown in Fig. 7, are overlain in white on the directional derivative of the bathymetry calculated with respect to the site 2 bistatic source location and the receiver location in the middle of track 17. Only prominent (>10 dB above local average) and repeatable events that occur in at least 10 charts out of 49 are overlain. Scattering events of interest within the trapezoid do not orginate from the seafloor because the seafloor in this region is level. The returns are probably due to other scatterers in the water column or in the subbottom.
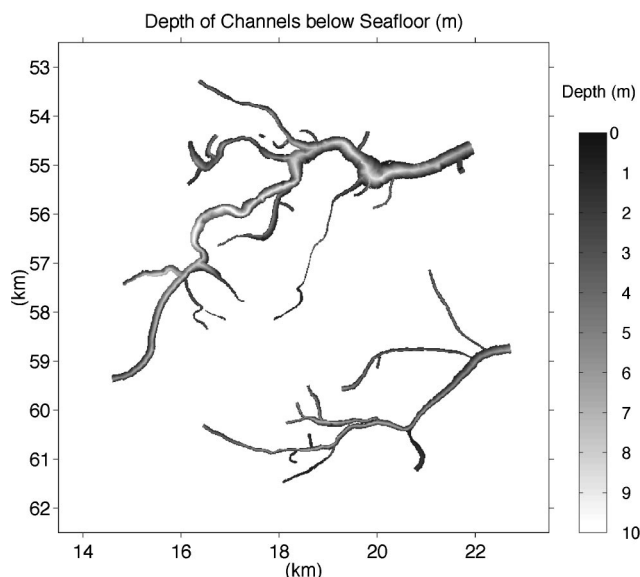
Depth of Channels below Seafloor (m)

FIG. 10. Most recent interpretation[27] of the depth of the buried river channels at site 2 below the water–sediment interface. This interpretation is based on geophysical survey of August 2001[26] at site 2.

river channels found in this area from the geophysical survey in August 2001.

The trace of the buried river channels from Fig. 10 is overlain on the hotspot consistency chart for track 17 in Fig. 12. From Fig. 12, we observe that some of the prominent scattering events appear to coincide with the location of the newly discovered buried river channels. But the rest, especially the clutter in the south of the trapezoid, do not coregister. Possible source of scattering for these unidentified clutter events are discussed in Sec. V.
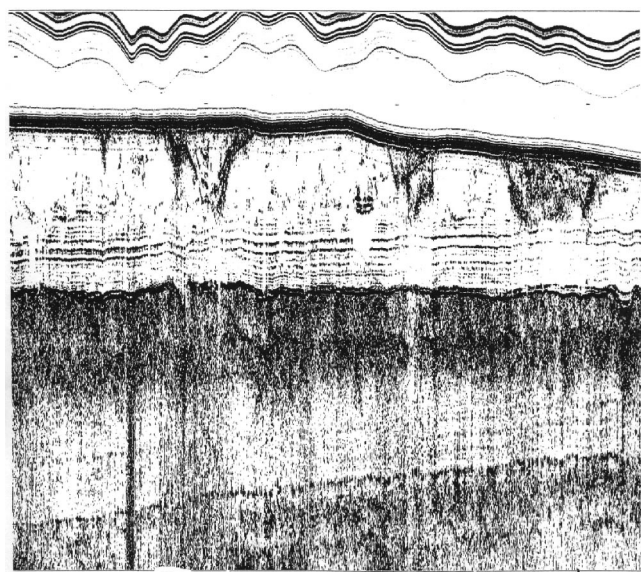

FIG. 11. Deep-tow subbottom chirp profile from the geophysical survey of August 2001[26,27] at site 2 showing three buried river channels discovered in the vicinity of the prominent and discrete scattering events observed at this site as shown in Fig. 7. Some of these channels at site 2 shoal close to the water–sediment interface and are less deeply buried than those at site 1. These river channels are located between 39° 1.3684′N, 73° 2.9619′W and 39° 2.2878′N, 73° 2.9624′W.

1. Temporal and spatial variability of clutter

The trapezoidal region in Figs. 6–8 that registered strong scattering events on tracks 17 and 14 also registered many clutter events with significant temporal and spatial variability over the course of the experiment. In general, these clutter events were found to be consistently observable over hours, but not longer than a day.

Apart from tracks 14 and 17, scattering events in the region within the trapezoid were also registered on track 23x where the data were collected on the same day as tracks 14 and 17. Figure 13 shows the hotspot consistency image composed of bistatic LFM transmissions along track 23x. We observe scattering events within the trapezoid, as well as returns from the calibrated targets. Fewer bistatic signals were transmitted along track 23x than in tracks 17 or 14, as noted in the figure.

No high-level clutter is observed within the trapezoid during track 18, a day before track 17, as shown by the hotspot consistency chart for track 18 in Fig. 14. Track 18 has the same source depth of 55 m and same mean receiver array depth of 42 m, but a different location and orientation from track 17. The scattering events originating from the calibrated targets are prominent in Fig. 14. Only sidelobe leakage from the calibrated targets in the endfire direction appears within the trapezoid.

Figures 15(a)–(d) show data from four tracks with similar centers, but different orientation from tracks 17 and 14. (Note that Fig. 15 is displayed after Fig. 16.) These data were collected within a half-day period 4 days after tracks 17 and 14 were run. Several prominent clutter events occur in the trapezoidal region in Figs. 15(a) and (c). However, little or no clutter is observed in that region in Figs. 15(b) and (d). This figure shows that clutter events in and out of the trapezoid are highly variable functions of array orientation, time, or both. Since none of the individual tracks were repeated, the purely temporal variability cannot be isolated in this experiment. No returns can be seen from the calibrated targets in the later measurements because they deflated within days and were no longer functional.

2. Statistical analysis of clutter repeatability inside and outside of areas occupied by buried river channels at site 2

Clutter data from all site 2 tracks over the region where the subbottom has been profiled are analyzed statistically. The goal of this analysis is to compare the frequency of occurrence of repeatable clutter inside and outside of regions occupied by buried river channels. For each track, a hotspot consistency subimage covering a box of dimension 9.5×10.5 km^2 containing the buried river channels is used in the analysis. This region is the area within the yellow box in Fig. 12. The area occupied by the buried river channels within this box is approximately 5.8% of the total area of the box. An area surrounding the targets of width 1.7×2.2 km^2 is excluded from the analysis. For each track with index n, the number of pixels $T_n(10\%)$ with hotspots that are repeatable in at least 10% of the total number of images N_n along the track is computed for the box. The number of these pixels $C_n(10\%)$ that chart within buried river channels is next com-
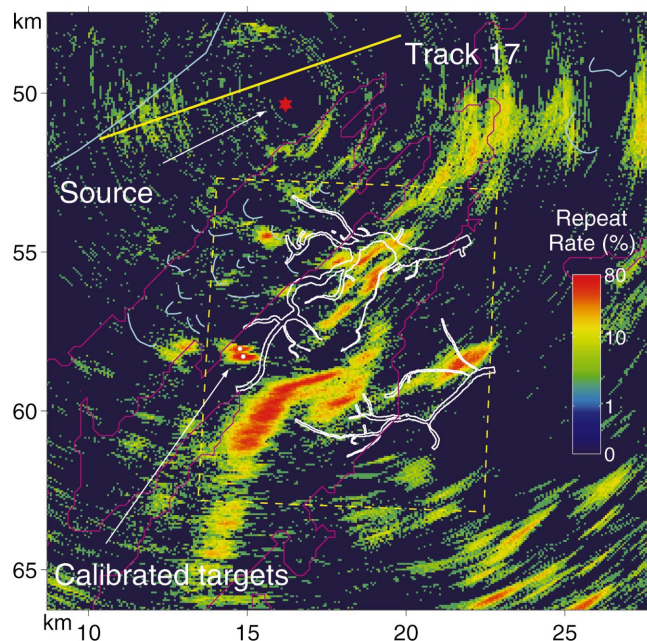
Ratilal *et al.*: Acoustic clutter reconnaissance experiment 2001

FIG. 12. Hotspot consistency chart for track 17 with white overlay showing the trace[27] of buried river channels discovered at site 2. This interpretation of the river channel is based on data from the August 2001 geophysical survey[26,27] within the yellow dashed box, acquired using chirp subbottom profiling systems. Some of the prominent scattering events appear to correspond with the newly discovered river channels. Some of the events to the south, however, do not correlate with any known geologic feature in this region. This indicates that some of the prominent acoustic returns measured at site 2 are probably caused by other objects in the water column. Large and densely populated schools of fish were measured[34,35] around the 80-m water depth contour (shown in pink line) of the STRATAFORM area and are a possible cause of some of the prominent clutter returns at this site.

FIG. 14. Hotspot consistency chart for 47 bistatic transmissions along track 18. Data for track 18 were collected a day before that on track 17. Prominent events >20 dB above the background are registered from the two calibrated targets approximately 8.5 km to the south of the source. No high level scattering event can be detected within the trapezoid (yellow-dashed line) in this figure. The 80-m bathymetric contour is shown in pink. (Date: 30 April, time: 15:30:00Z to 16:45:00Z, mean source depth: 55 m, mean receiver depth: 42 m, array heading: 340°.)
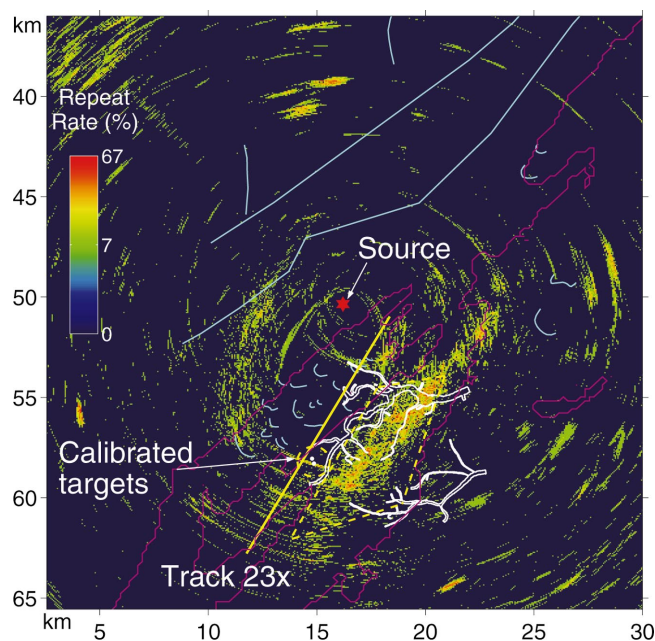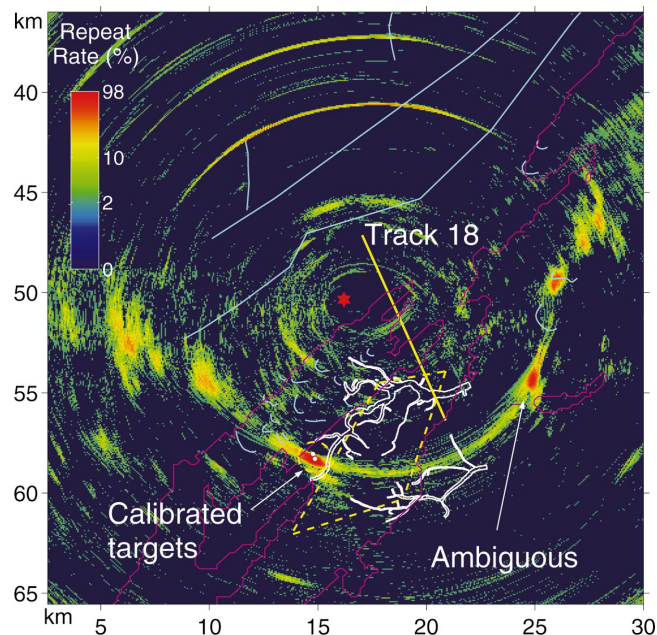

FIG. 13. Hotspot consistency chart for 15 bistatic transmissions along track 23x. Data for track 23x were collected on the same day as track 17. Prominent events >20 dB above the background are registered from the two calibrated targets approximately 8.5 km to the south of the source. Scattering events located within the trapezoid (yellow-dashed line) can be observed for track 23x, similar to that on tracks 17 in Fig. 7. The 80-m bathymetric contour is shown in pink. (Date: 1 May, time: 21:45:00Z to 23:10:00Z, mean source depth: 55 m, mean receiver depth: 43 m, array heading: 209°.)
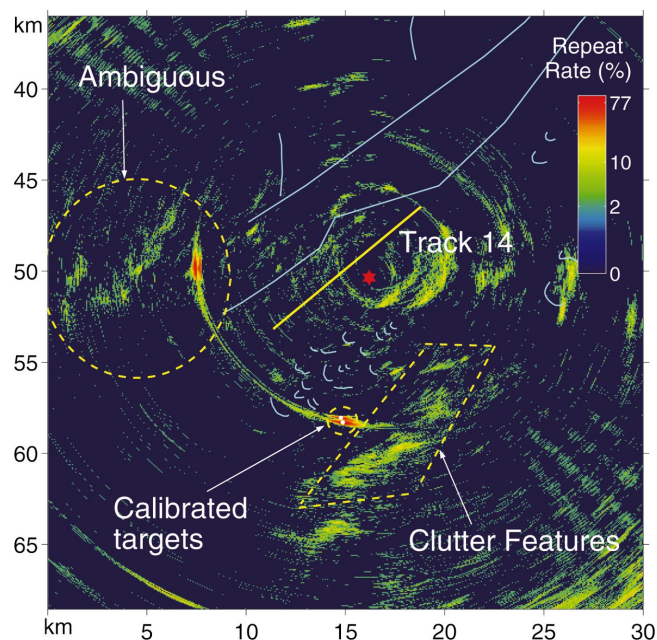

FIG. 16. Hotspot consistency image for 46 bistatic transmissions along track 14. Prominent scattering events with levels 10 dB above the background co-register with the location of the calibrated targets in most of the images. Scattering events originating from clutter features within the trapezoid are not registered as consistently along track 14. It should be noted that track 14 had a shallower receiver depth than track 17 in Fig. 7. This hotspot image shows that measurement of clutter varies with time and may also depend on receiver depth. (Date: 1 May, time: 10:30:00Z to 11:52:00Z, mean source depth: 55 m, mean receiver depth: 22 m, array heading: 226°.)
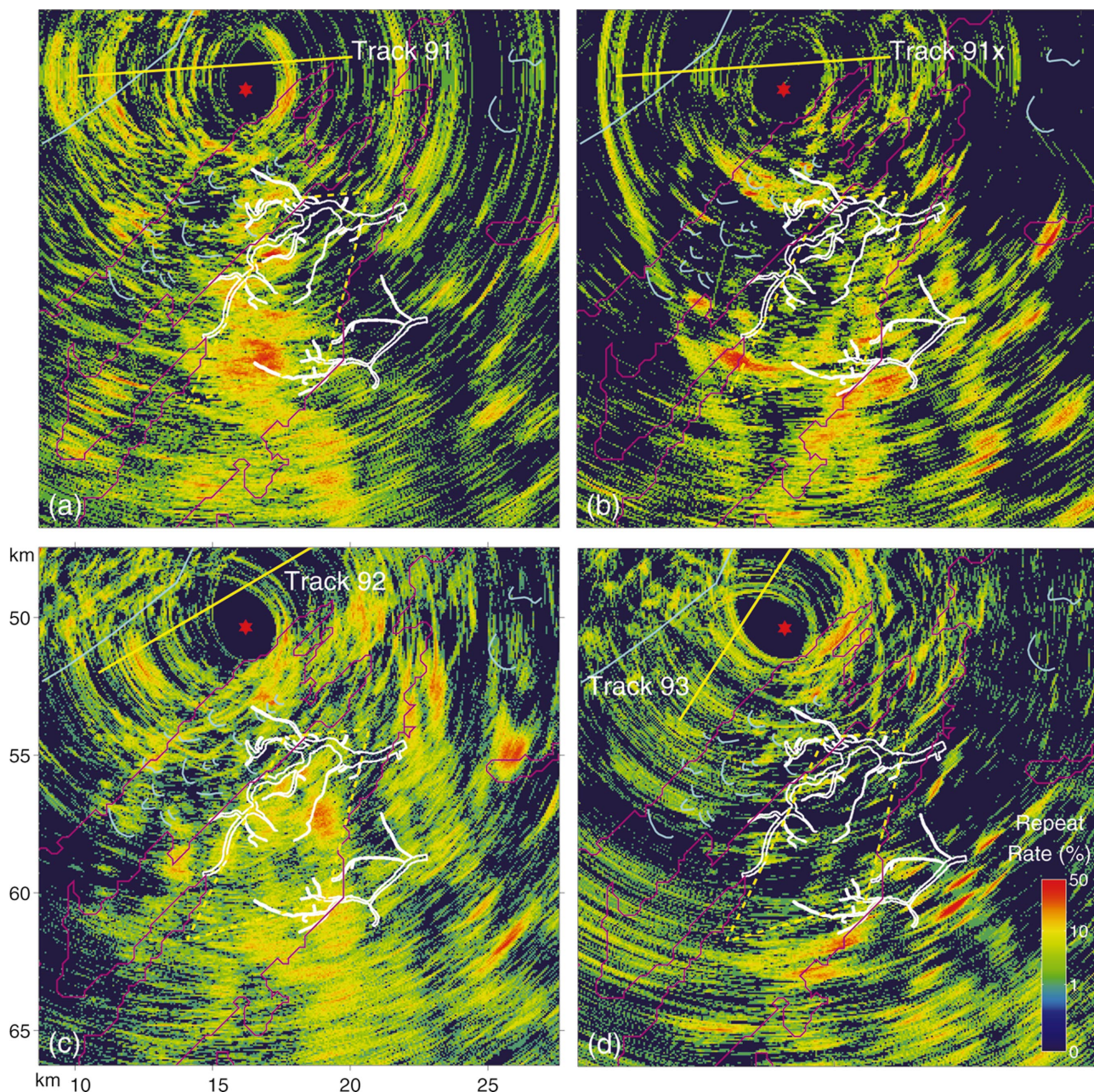
FIG. 15. Hotspot consistency charts for (a) 60 bistatic transmissions along track 91 with array heading 268.5°, (b) 42 bistatic transmissions along track 91x with array heading 270°, (c) 94 bistatic transmissions along track 92 with array heading 49°, and (d) 74 bistatic transmissions along track 93 with array heading 208.5°. Data for these tracks were collected on the same day. We observe that the scattering events within the trapezoid (yellow-dashed line) show temporal and spatial variability. The calibrated targets at site 2 had deflated during this measurement and are hence not detectable. The 80-m bathymetric contour is shown in pink. [(a)–(d) Date: 5 May, mean source depth: 35 m, mean receiver depth: 36 m.]

puted. The ratio of these quantities defined by $[C_n(10\%)/T_n(10\%)] \times 100\%$ gives the percentage $P_n(10\%)$ of repeatable clutter at 10% repeatability or more within the buried river channels. The percentage $P_n(20\%)$ is also calculated for clutter that is repeatable in at least 20% of the total number of images along the track. The results are shown in Table I. The frequency of occurrence of repeatable clutter within buried river channels has a mean from 2.3% to 4.9% and standard deviation from 1.8% to 4.3%. This frequency of occurrence of clutter within the buried river channels differs by less than a standard deviation from the area occupied by the channels in the subimage of 5.8%. This im-

plies that to within the errors of the statistical analysis, there is no evidence that the repeatable clutter favors buried river channel locations over the nonchannel locations.

3. Possible variation of clutter with receiver depth

Figure 16 shows the hotspot consistency chart for the 46 bistatic transmissions along track 14. Prominent and discrete events register at the locations of the calibrated targets in 41, or 89%, of the images. Scattering events from features within the trapezoid, however, are prominent with levels of more than 10 dB above the background in at most 7, or 15%, of

TABLE I. Frequency of occurrence of repeatable clutter within the yellow box at site 2 shown in Fig. 12. Buried river channels occupy 5.8% of the area of this box. The $M = 11$ tracks listed below are the only ones that transmitted bistatic LFM signals at site 2. Column 2 indicates N_n, the total number of images along track n, used to form the hotspot consistency chart over the box area. Columns 3 and 4 indicate $P_n(10\%)$ and $P_n(20\%)$ which are the percentages of repeatable clutter with at least 10% and 20% repeatability, respectively, that are charted within the buried river channels for each track. The unweighted mean percentages of repeatable clutter with at least 10% and 20% repeatability charted within buried river channels are calculated by taking the average of $P_n(10\%)$ and $P_n(20\%)$ respectively over all M tracks. The unweighted mean and standard deviation do not take into account the variation in the total number of images along each track. The weighted mean and standard deviation account for variations in the total number of images along each track.

Track index, n	Track name	N_n	$P_n(10\%)$ (%)	$P_n(20\%)$ (%)
1	13	46	3.2	12.0
2	14	46	2.0	0.0
3	17	49	4.4	3.2
4	18	47	4.9	10.8
5	19	9	9.3	8.2
6	20	9	4.9	3.4
7	23x	15	8.5	10.1
8	91	60	4.2	2.6
9	91x	42	3.2	3.3
10	92	94	4.5	0.0
11	93	74	1.2	0.5
Unweighted mean $\bar{P} = \dfrac{1}{M}\displaystyle\sum_{n=1}^{M} P_n$			4.6	4.9
Unweighted standard deviation $\sigma = \sqrt{\dfrac{1}{M}\displaystyle\sum_{n=1}^{M}(P_n - \bar{P})^2}$			3.7	3.7
Weighted mean $\overline{P'} = \dfrac{1}{\sum_{n=1}^{M} N_n}\displaystyle\sum_{n=1}^{M} N_n P_n$			2.3	4.3
Weighted standard deviation $\sigma' = \sqrt{\dfrac{1}{\sum_{n=1}^{M} N_n}\displaystyle\sum_{n=1}^{M} N_n(P_n - \overline{P'})^2}$			1.8	4.3

the images along track 14. These images were acquired when NRV *Alliance* was located towards the south-western end of the track. Clutter events measured while the NRV *Alliance* was in the north-eastern part of track 14 were less prominent within the trapezoid. Tracks 17 (shown in Fig. 7) and 14 are located at roughly the same range from the calibrated targets and the objects located within the trapezoid, but they differ in their orientation by approximately 10°. Data for these two tracks were collected on the same day, approximately 2 h apart. The receiver array was at a shallower depth in the water column of about 22 m on track 14, while it was deeper at 42 m depth on track 17. The bistatic source depth of 55 m and location did not change. These images show that variation of receiver depth may have caused substantial differences in our ability to image the clutter events within the trapezoid. Imaging of the calibrated targets is more stable with respect to changes in receiver depth. It is also highly-likely that the scatterers causing clutter may have evolved over this time leading to the observed differences in our ability to image them.

Note that the sound speed in the water column close to the location of the clutter features and calibrated targets has a maximum around 40- to 50-m depth due to a protruding filament of warm Gulf stream water as discussed in the appendix. This profile is downward refracting for a source depth of 55 m. Better detection can be obtained of scatterers located near the bottom for a deep receiver than a shallow receiver The two calibrated targets are tall cylindrical tubes that span close to half the water column from 32- to 62-m depth which allows them to be detected much more readily regardless of the sound speed profile or receiver depth.

B. Site 3

At this site, patches of returns stretching over 35 km in range are imaged near the 100-m water depth contour on tracks 61 and 62 as seen in Figs. 17(a) and (b) respectively. Comparing Figs. 17(a) and (b) enables ambiguity about the line array to be resolved. The true location of the returns is to the south-west in both charts. It is noteworthy that the shelf break front in this region where the warmer slope water intersects the seafloor also occurs along bathymetric contour with similar water depth (see the appendix). The significance of the shelf break front to acoustic scattering is discussed further in Sec. V.

Two seafloor features are also imaged at site 3. Figures 18(a) and (b) show the hotspot consistency images formed from data acquired along tracks 61 and 62, respectively. For these particular images, levels 10 dB above the local average over an area 2.7×2.7 km^2 are selected as peaks. The iceberg scour on the seafloor about 5 km away from the source is imaged on both tracks repeatedly. This particular iceberg scour is the only one imaged in the experiment. Scattering from the wall of the Hudson Canyon more than 30 km away from the source and receiving array is also registered as seen

J. Acoust. Soc. Am., Vol. 117, No. 4, Pt. 1, April 2005   Ratilal *et al.*: Acoustic clutter reconnaissance experiment 2001   1989

Redistribution subject to ASA license or copyright; see http://acousticalsociety.org/content/terms. Download to IP: 18.38.0.166 On: Mon, 12 Jan 2015 18:13:16
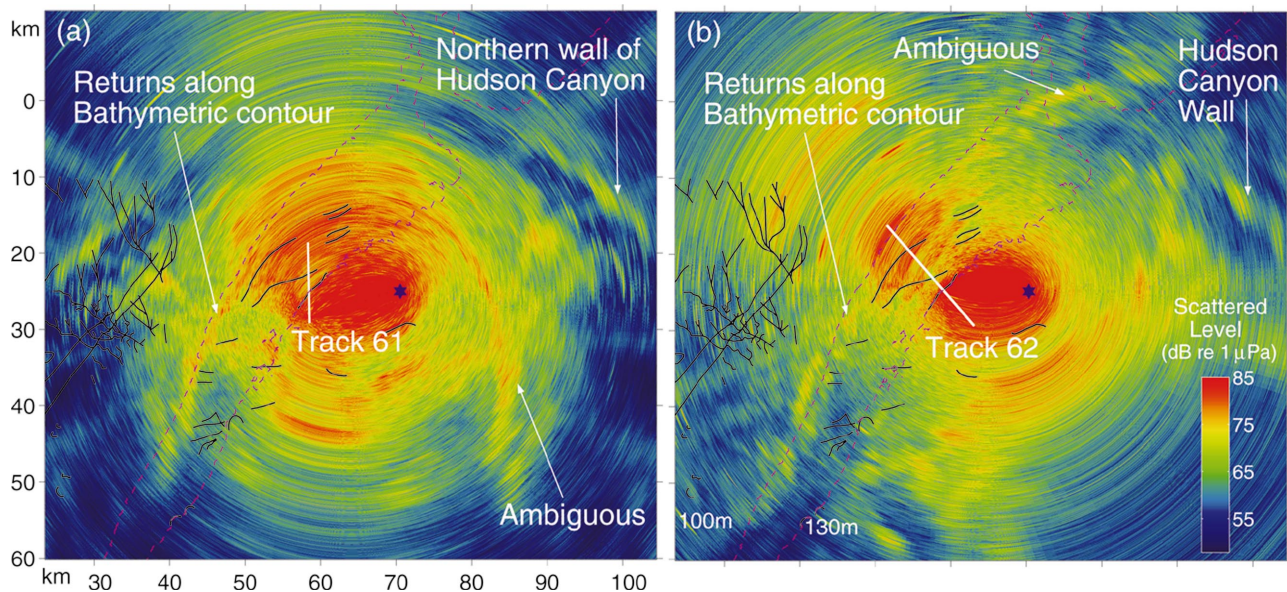
FIG. 17. Single-ping bistatic wide-area images from tracks 61 and 62 at site 3. Patches of scattered returns stretching over 30-km range and that line up with the 100-m water depth contour were imaged in this region. Comparing (a) and (b) allows the receiver line array's left-right ambiguity to be resolved. [(a): Track 61, date: 2 May, ping time: 12:11:40Z, transmission: 2-s duration LFM from 390 to 440 Hz, mean source depth: 84 m, mean receiver depth: 60 m, array heading: 358°. (b) Track 62, date: 2 May, ping time: 16:08:20, transmission: 2-s duration LFM from 390 to 440 Hz, mean source depth: 84 m, mean receiver depth: 34 m, array heading: 133°.]

in Figs. 17 and 18. Some of the patches of returns along the bathymetric contour are also visible in the hotspot consistency image in Fig. 18.

C. Site 1 with statistical analysis of clutter repeatability in and out of buried river channels

Site 1 was the focus of previous geophysical surveys where extensive networks of buried river channels were mapped and characterized prior to the ACRE.[14,15] Additional geophysical surveys were conducted after the ACRE to provide better characterization of the channel morphology.[26,28]

During the first few days of the ACRE, a large number of tracks were traversed by RV *Alliance* at various ranges and azimuths from the buried river channels at site 1 shown in Fig. 19, to explore possible scattering and hence imaging of these channels. Prominent clutter events were observed
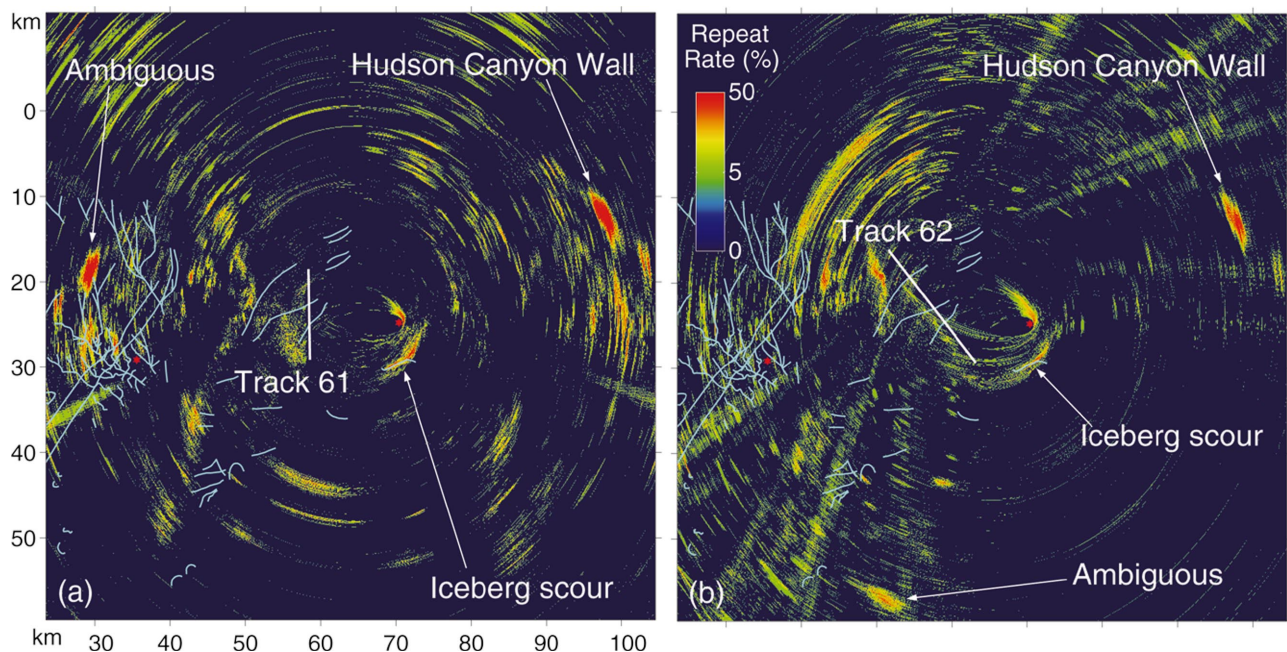

FIG. 18. Hotspot consistency charts from (a) 15 bistatic LFM transmissions along track 61, and (b) 21 bistatic transmissions along track 62 and at site 3. The figure displays the number of images that register a strong scattering event >10 dB above the local average within 2.7×2.7 km² area of a given pixel location. Comparing (a) and (b) breaks the receiver line array's right–left ambiguity. It registers prominent scattering from the walls of the Hudson Canyon located to the west in both figures, as well as scattering from the iceberg scour close to the location of the bistatic source. [(a) Track 61, date: 2 May, mean source depth: 84 m, mean receiver depth: 60 m, array heading: 358°. (b) Track 62, date: 2 May, mean source depth: 83.8 m, mean receiver depth: 34 m, array axis: 358°.]
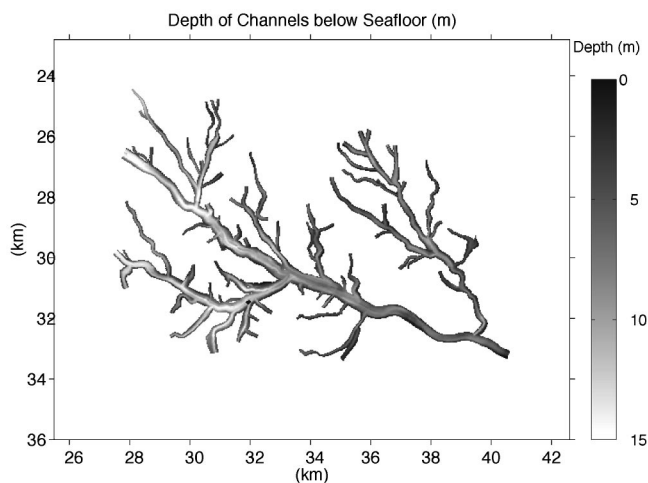
FIG. 19. Most recent interpretation[28] of the depth of the buried river channels at site 1 below the water–sediment interface. This interpretation is based on geophysical surveys at site 1.

throughout the region. Some of the clutter events intersect with the buried river channels. However, the registration of the clutter with the channels could not be maintained from one track to the next.

Towards the end of the ACRE, a more controlled data collection procedure was adopted where higher temporal and spatial sampling were employed to study clutter repeatability. Bistatic sonar data were collected along six tracks numbered tracks 81 to 86, located within 5-km range of the buried river channels. These tracks had the same track center but with orientations that differed by 15° from one track to the next. Rapid transmissions were made of the same LFM waveform for all these tracks. This allowed a large number of acoustic images to be captured over small variations in receiver azimuths of approximately 1°. (This angular variation is within a scatter function lobe for objects smaller than 200 m.)

Figures 20(a)–(f) show the hotspot consistency images from tracks 81–86, respectively. Figures 21(a)–(f) provide a zoomed version of Figs. 20(a)–(f) in the vicinity of the channels where the subbottom data have been collected and analyzed. In these figures, the traces of the most recent interpretation[28] of the river channel morphology at site 1, shown in Fig. 19, are overlain as white lines. Some prominent hotspots occur within the buried river channels, as in Figs. 21(e) and (f), while many other prominent hotspots occur outside of the channels, as in Fig. 21(c).

From Figs. 20(a)–(f), we do observe many more extended hotspots to the east and south-east in these images. These hotspots are consistently observable in several tracks and seem to occur along a bathymetric contour that is deeper but parallel to the 100-m water depth contour. These images should be compared with Fig. 17 where the returns line-up close to the 100-m water depth contour.

Several other prominent and discrete scattering events close to the 100-m water depth region were also imaged at site 1 as shown in Figs. 22(a) and (b). These images also show how a hotspot consistency chart can be used to resolve ambiguity. In the single ping image of Fig. 22(a) from track 73, a set of prominent and discrete scattering events are

charted to the north-west and another set of more elongated events to the south-east. Only one of these is the true set of scattered returns while the other is ambiguous. From Fig. 22(b), which shows the hotspot consistency chart for the track, the events from the south-east are consistently charted to the same area, leading to a strong reinforcement of these events in the hotspot chart. The events to the north-west are distributed over a wide area in the hotspot chart with little repeatability, showing that these events are the ambiguous ones. The true scattered returns therefore originate from the south-east in the region with water depth of between 80 to 100 m. Geophysical surveys at the location of these extended clutter returns did not find any subbottom features.[26]

The measured clutter on all the tracks at site 1 is also statistically analyzed to compare the frequency of occurrence of repeatable clutter inside and outside of buried river channels. The analysis is similar to that done at site 2 and discussed in Sec. IV A 2. The area used in the analysis is the full region shown in Fig. 19 of 17.2×13.3 km^2, which is the same as that in Figs. 21(a)–(f). The area occupied by the buried river channels within this box is approximately 9% of the total area of the box. The results are shown in Table II. The means of between 13% to 15% and standard deviations of between 7% to 14% show that there is no statistically significant difference between the frequency of occurrence of repeatable clutter charted within areas occupied by buried river channels and that charted outside of areas occupied by channels. This finding is similar to that at site 2.

V. SUMMARY AND DISCUSSION

At all the three sites investigated in the New Jersey Strataform area, a large number of clutter events were imaged throughout the experiment. Many often persisted along a track. These events were imaged in near-real-time over wide areas extending roughly 40 km in range from the bistatic sonar. Most of the clutter events were measured in areas where the bathymetry is locally level with slopes <0.5°. At site 2, these scattering events are sometimes as prominent and consistent as those from the calibrated targets deployed at a similar range from the bistatic sonar. Without prior knowledge, it would be impossible to distinguish the targets from these features.

Some of the high-level clutter events intersected buried river channels at sites 1 and 2. In general, the registration of clutter events with the buried river channels at a given location could not be maintained over variations in track orientation. Since none of the tracks were repeated, it is unknown whether or not the registration of the clutter for a given track with the channels is repeatable over time.

We consider two plausible causes for the variability in measured clutter with changes in track orientation. If the measured clutter is caused by scattering from geologic features of the subbottom such as buried river channels, its variability shows that the scattering process is highly dependent on the bistatic location and orientation of the source and receiver array relative to the geologic features. An analogy can be drawn with the "glints" observed on a spoon. Due to the curved surface of the spoon, the glints on a spoon migrate when the bistatic orientation of the observer or light
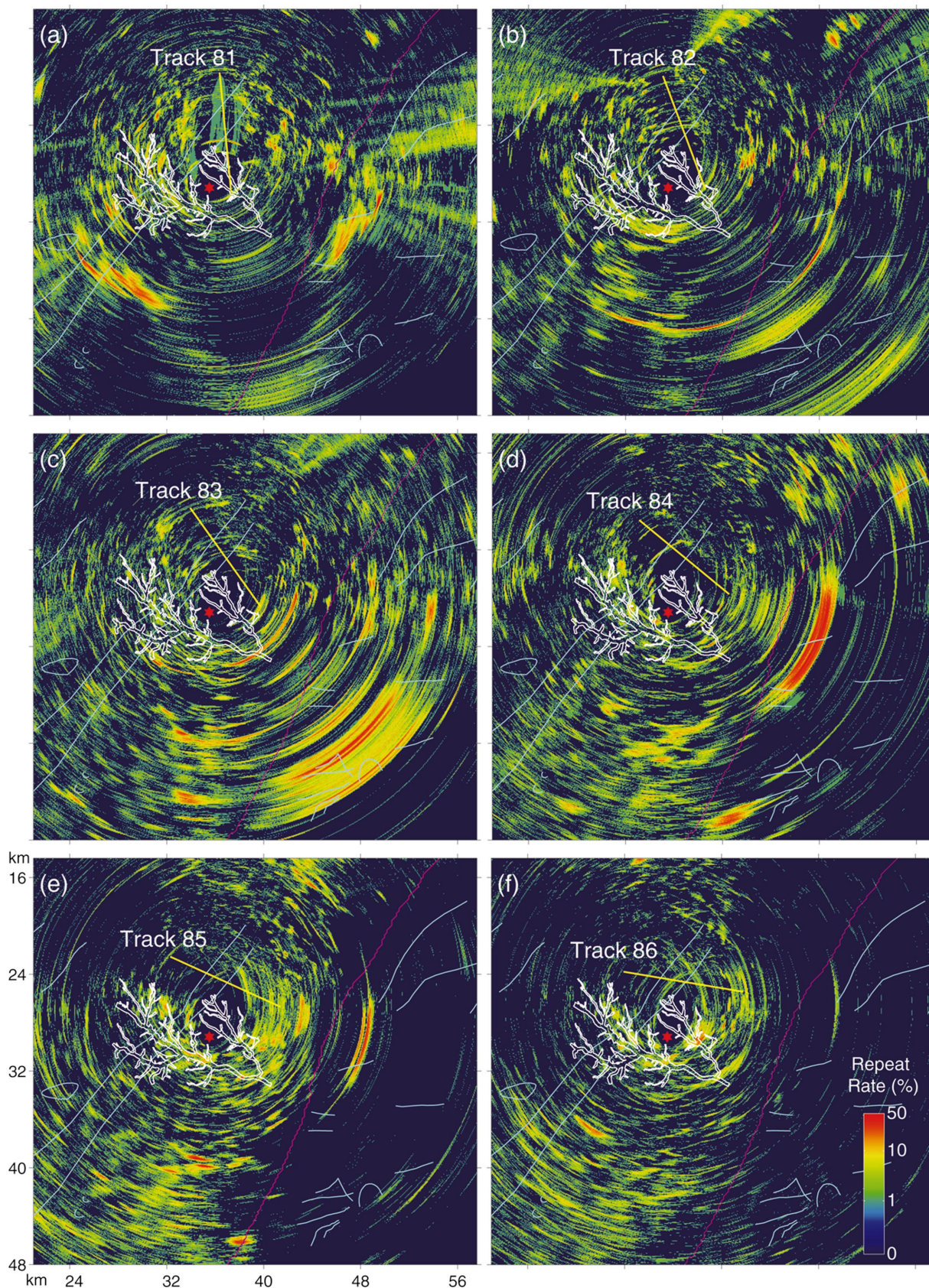
FIG. 20. Hotspot consistency chart for (a) 89 bistatic transmissions along track 81 with array heading 350°, (b) 78 bistatic transmissions along track 82 with array heading 154°, (c) 94 bistatic transmissions along track 83 with array heading 327°, (d) 73 bistatic transmissions along track 84 with array heading 122°, (e) 87 bistatic transmissions along track 85 with array heading 293°, and (f) 79 bistatic transmissions along track 86 with array heading 97°. The 100-m bathymetric contour is shown in pink. The most prominent and repeatable clutter, consistently observable in several of the tracks, occur in waters that is a little deeper than 100 m. The region where the buried river channels are shown is the only region where subbottom data have been collected and analyzed. There may be subbottom features in other regions shown in this figure, but the subbottom geologic data have either not been collected or not analyzed. [(a)–(d) Date: 4 May, mean source depth: 41 m, mean receiver depth: 35 m.]
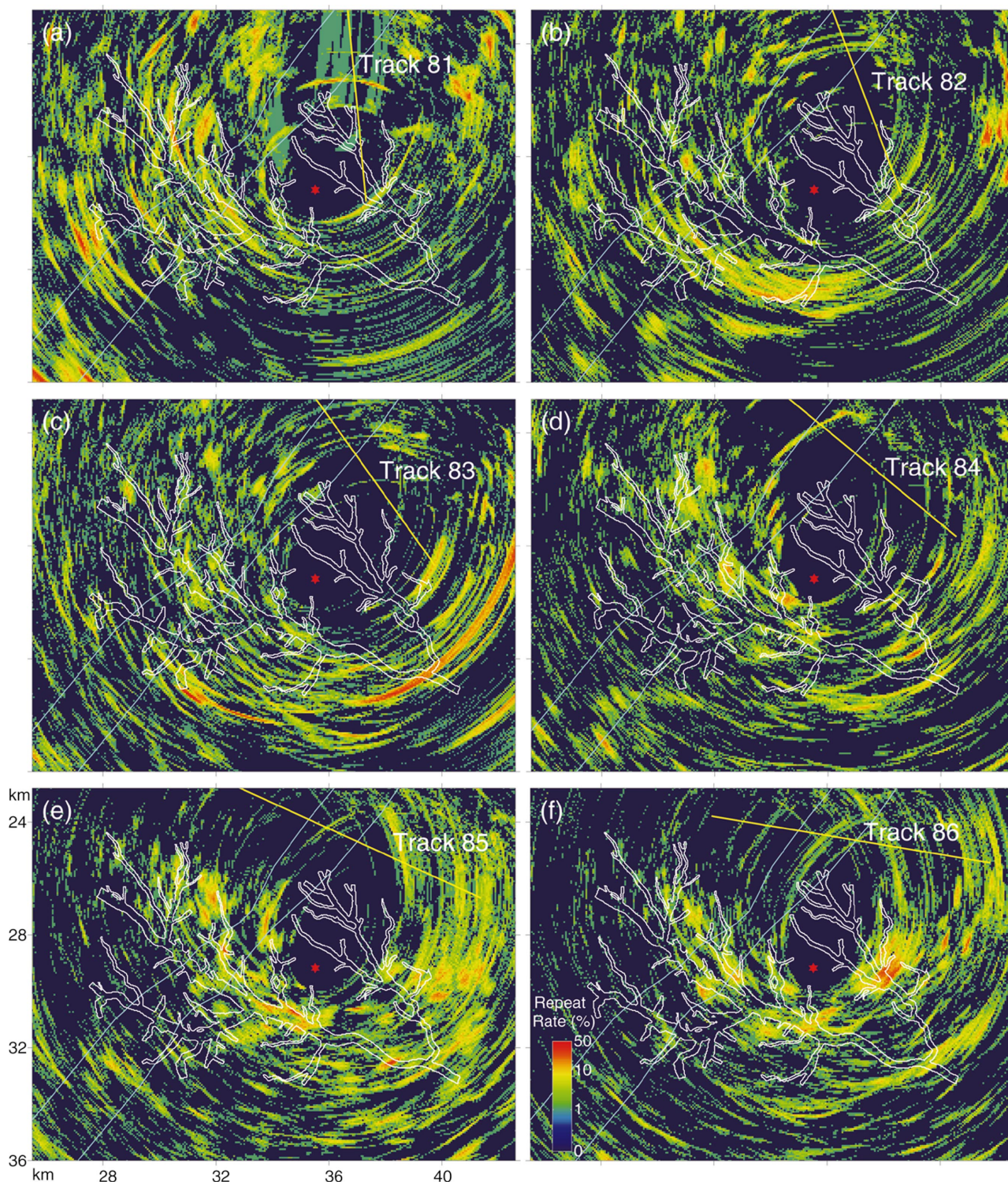
FIG. 21. (a)–(f) are similar to Fig. 20 but are zoomed in around the channels at site 1. The clutter registration with the channels changes with the orientation of the tracks which were done at different times of the day.

source changes.[29] The projected area of the imaged feature within the cross-range resolution of the measurement system changes with the bistatic orientation of the system relative to the feature. Bistatic aspects that lead to large projected areas would produce the strongest returns. In deep water, this is the case with deterministic reverberation from scarps on the Mid-Atlantic Ridge. The scattering strength of the scarp was found to be proportional to the projected area of the scarp

along the path from target to the bistatic source and receiver.[8–10] Another possibility is that the clutter arises from objects moving around in the water column. This could account for the highly spatial and temporal variability observed in the measured clutter. Regardless of the origin of the clutter, returns in a waveguide also fluctuate as a result of propagation effects due to interference between the modes. The strength and consistency of the clutter measured at site 2 was

J. Acoust. Soc. Am., Vol. 117, No. 4, Pt. 1, April 2005

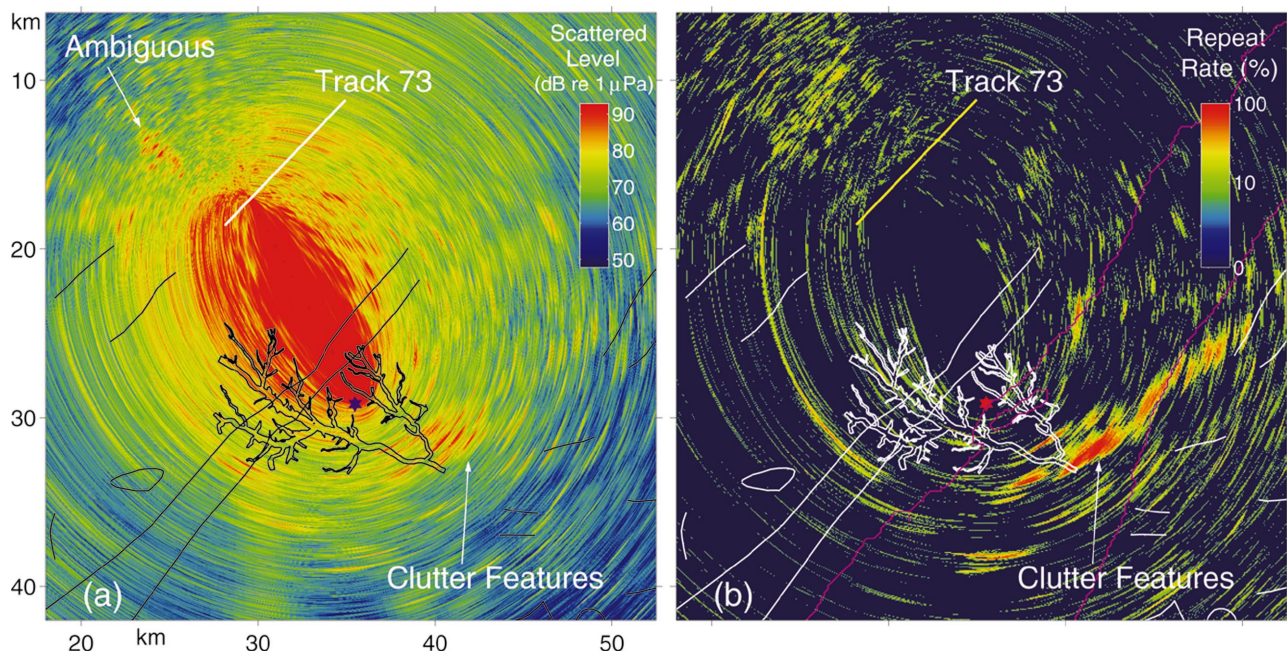Ratilal *et al.*: Acoustic clutter reconnaissance experiment 2001   1993

FIG. 22. (a) Single-ping bistatic wide-area image from track 73 at site 1. (b) Hotspot consistency chart for 12 bistatic transmissions along track 73 at site 1. In (a), a set of prominent and discrete scattering events has been charted to the north-west and another set of more elongated events have been charted to south-east. Only one of these is the true scattered return from the features while the other is ambiguous. Comparing (a) and (b) shows that the events to the south-west are the true returns. These returns do not coincide with any known geologic features, but are contained within the 80- to 100-m bathymetric contour (pink lines) of the STRATAFORM area at site 1. [Date: 3 May, (a) ping time: 16:28:35Z, transmission: 2 s duration LFM from 390 to 440 Hz. (a) and (b) Mean source depth: 41 m, mean receiver depth: 38 m, array heading: 220°.]

also found to vary with receiver depth and could be due to effects of the sound speed profile in the water column.

It should be noted that statistical analysis of the measured clutter at sites 1 and 2 in regions where the buried river channels have been mapped show that there is no significant difference between the rate of repeatable clutter per unit area charted within areas occupied by buried river channels and that charted outside of areas occupied by channels.

Seafloor features, such as the one iceberg scour and the large wall of the Hudson Canyon, are the only geologic features consistently imaged in the acoustic experiment. The one iceberg scour was detected at approximately 5-km range while the Canyon wall was imaged at about 30 km from the bistatic sonar at site 3. The returns from the Canyon wall are strong, but extended and not target-like in appearance.

Many of the prominent clutter events at all three sites occurred in the region along bathymetric contour between 80- and 120-m water depth. This is roughly the region where the warmer slope water mixes with the cooler shelf water in the New Jersey Strataform area as discussed in Appendix A.

One possibility for the source of unidentified clutter measured at sites 1–3 is scattering from fish.[30–33] Fish are known to exist in tight schools about 5 m off the bottom in the STRATAFORM area with 80- to 120-m water depth.[34,35] This is where the the shelf break front exists which contains nutrients and is a source of food that attracts the fish schools. This possibility of fish schools causing clutter in long range sonar has been shown to be theoretically plausible[30–33] and has also been observed experimentally.[36] When fish congregate together to form large and densely populated schools, they can scatter either coherently or incoherently, leading to returns that stand significantly above the diffuse reverbera-

tion background.[32,33] This has been observed experimentally where such fish schools were found to be distributed in fan-shaped patterns.[36]

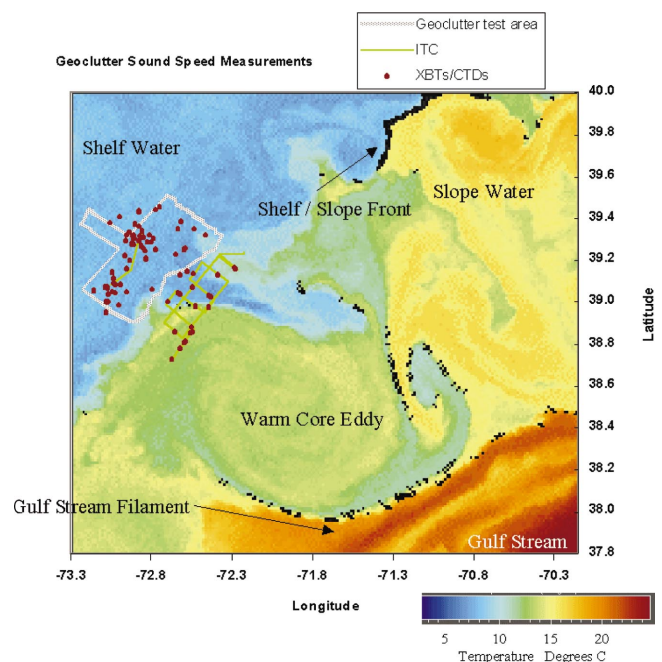Another possible origin for the unidentified clutter is

FIG. 23. Satellite image of the sea surface temperature off the New Jersey Coast on 30 April 2001. The oceanography in the region is governed by the interation between the cooler shelf water (in blue), the warmer slope water (in yellow), and much warmer water from the gulf stream (in brown). Also visible is a warm core eddy (in green). Oceanographic data were collected using XBTs, CTDs, and an instrumented tow cable (TC) that allows almost continous measurement of temperature along a tow cable.

1994   J. Acoust. Soc. Am., Vol. 117, No. 4, Pt. 1, April 2005

Ratilal et al.: Acoustic clutter reconnaissance experiment 2001

TABLE II. Same as Table I but calculated for the tracks and the box with the full area in Fig. 19 at site 1. Buried river channels occupy 9.0% of the area of this box. There are a total of $M = 21$ tracks at site 1 that transmitted bistatic LFM signals.

Track Index, n	Track name	N_n	$P_n(10\%)$ (%)	$P_n(20\%)$ (%)
1	1c	9	15.9	17.6
2	1x	14	22.9	31.7
3	2	11	11.4	9.5
4	3	16	9.4	7.4
5	4	15	3.3	3.3
6	5	15	26.5	41.6
7	7	15	13.4	9.0
8	8	14	15.5	15.3
9	11	12	8.9	7.2
10	12	13	12.4	15.5
11	71	11	8.8	5.1
12	72	15	5.3	3.1
13	73	12	6.0	4.8
14	74	12	7.4	6.5
15	75	18	12.9	9.9
16	81	89	8.5	3.1
17	82	78	7.2	0.0
18	83	94	7.5	7.0
19	84	73	7.7	0.0
20	85	87	23.6	45.5
21	86	79	30.3	43.1
Unweighted mean $$\bar{P} = \frac{1}{M}\sum_{n=1}^{M} P_n$$			12.6	13.6
Unweighted standard deviation $$\sigma = \sqrt{\frac{1}{M}\sum_{n=1}^{M}(P_n - \bar{P})^2}$$			7.3	14.0
Weighted mean $$\overline{P'} = \frac{1}{\Sigma_{n=1}^{M} N_n}\sum_{n=1}^{M} N_n P_n$$			13.5	15.4
Weighted standard deviation $$\sigma' = \sqrt{\frac{1}{\Sigma_{n=1}^{M} N_n}\sum_{n=1}^{M} N_n(P_n - \overline{P'})^2}$$			8.5	10.3

scattering from gas entrapments (pockets) within the sediment that have significant acoustic impedance contrast with the neighboring sedimentation.[37] There is, however, much debate over whether these pockets of gases can exist in the East Coast STRATAFORM area. None of the geophysical surveys found any evidence of gas pockets in this region. Gas pockets are therefore less likely to be the source of the measured clutter in comparison to fish schools that have been proven to exist in abundance in this region.

The temporal and spatial variability of the clutter events, along with resonance characteristic of the clutter, provide important clues regarding the identity of the scatterers and the physical mechanisms associated with the scattering process. Scattering from geologic features is expected to be repeatable at a given location as a function of time. Clutter from fish schools, on the other hand, is expected to evolve and change with both space and time as the fish congregate and disperse. Detailed theoretical analysis of the scattering from fish schools, buried river channels, the R-reflector, and reverberation from the sea bottom on the New Jersey Continental Shelf will be presented in a separate paper.

In order to condense the information contained in data from large numbers of transmissions along a track-line of the receiver ship, a "hotspot" consistency chart was derived from the images of individual transmissions along each track. The hotspot consistency chart displays the location and persistence of strong echo returns for transmissions along a track. In many instances, the hotspot charts provide significantly improved imaging of the clutter features. They are also useful for resolving the left–right ambiguity inherent in horizontal line array data when the bistatic range to the target is not much larger than the source–receiver separation. The hotspot charts also reduce charting errors due to waveguide dispersion since they combine information from a large number of transmissions.

The results of this experiment show that a low-frequency active sonar system can be used to remotely image the underwater environment over wide areas, at ranges spanning tens of kilometers, in continental shelf waters in near-real-time.
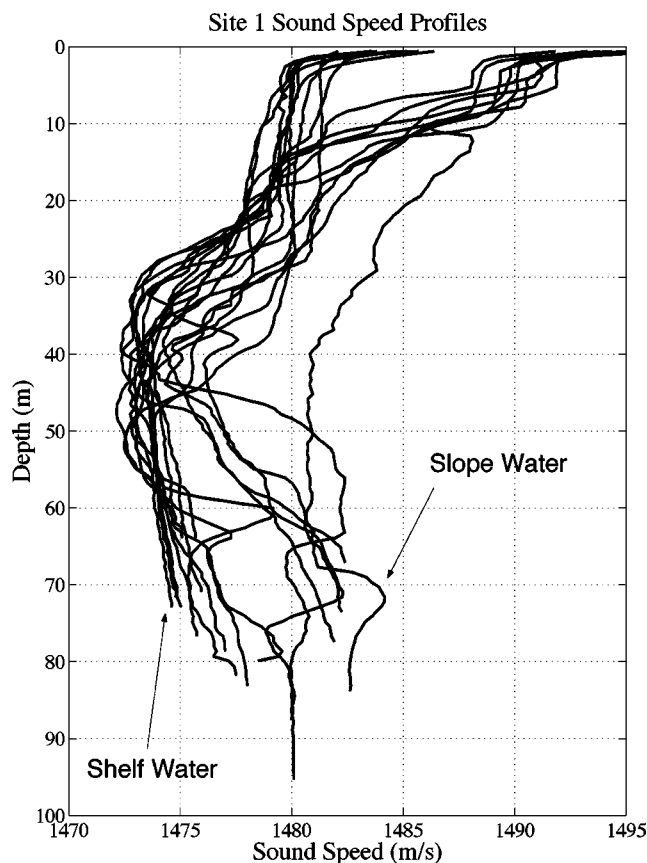
ACKNOWLEDGMENTS

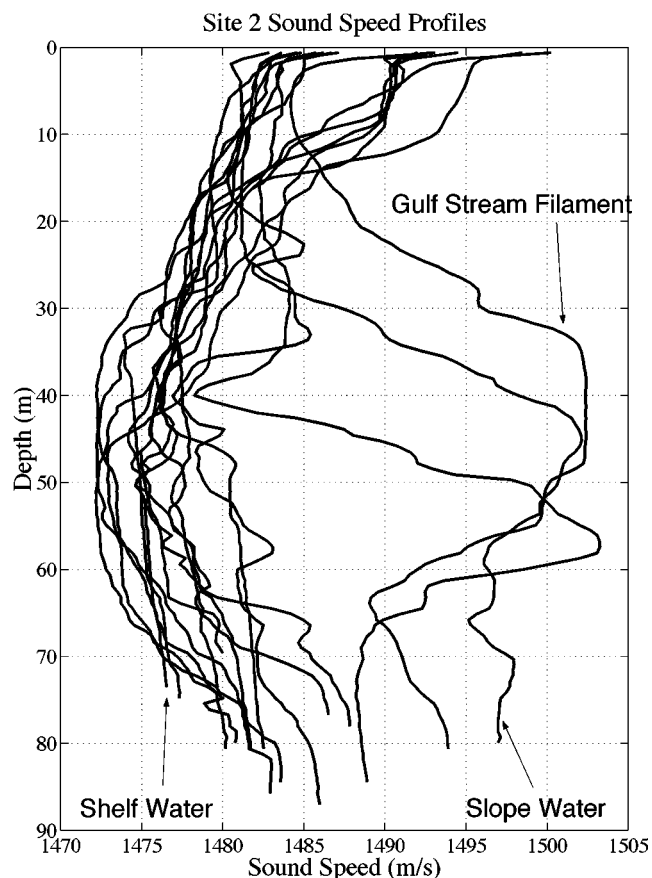FIG. 24. Measured sound speed profiles of the water column at site 1.

FIG. 25. Measured sound speed profiles of the water column at site 2.

cess. We would also like to thank Tommy Goldsberry for allowing us to use the MACE source and the engineering staff of the MACE Program for operation of the source during the experiment. We would like to acknowledge our colleagues at the University of Texas at Austin for providing us with geophysical support of the Program.

APPENDIX: STRATAFORM OCEANOGRAPHY

The East Coast STRATAFORM area has been fairly well characterized in general physical oceanography.[38–40] The dominant water masses consist of seasonally dependent shelf water, the surface mixed layer, and continental slope water (Fig. 23). The boundary between shelf and slope water is known as the shelf break front, and consists of a strong salinity gradient with seasonally dependent temperature gradients. Its shape and location are variable at different times of the year. Its surface expression is usually near the 200- to 1000-m bathymetric contour, while its intersection with the bottom frequently manifests up onto the outer continental slope, as shallow as the 70-m contour. Thus the shelf break front and slope waters influence the lowermost part of the water column in the test area. The upper part during the experiment was dominated by surface warming, the mixed layer, and a thermocline down to the mid-water-column shelf water.[41]

The oceanographic measurements during the experiment consisted of XBTs from both the RV *Endeavor* and NRV *Alliance*, 27 Seabird CTD casts from the RV *Endeavor*, and five deployments of the Instrumented Tow Cable,[42] a nearly
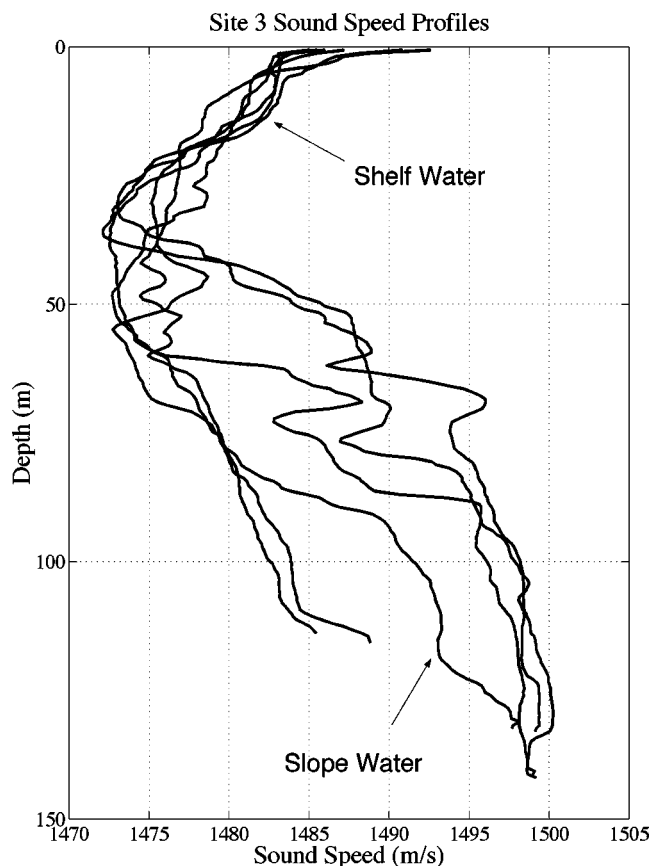

FIG. 26. Measured sound speed profiles of the water column at site 3.

continuous measurement device for temperature along a tow cable. In general, the measurements showed a sound speed profile with a moderately thin surface mixed layer (10 m or less), a thermocline of moderate gradient, to a temperature and sound speed minimum near 30- to 50-m depth (depending on the location) containing the ''cold pool'' of shelf water, below which was an increase in salinity and temperature associated with the shelf break front zone of mixing. The conditions have a tendency to channel the sound energy away from both the surface and bottom of the water column in the deeper portions of the area, and to allow better sound interaction with the bottom in areas shallower than 80 m.

Beyond this general physical oceanographic framework were two processes having a more variable effect on the sound speed structure. One was the existence of an unusually warm air mass over the area, causing near-surface warming continuously and gradually during the experiments, with a more pronounced effect in late afternoon. The second was the presence of a major (50 km diameter) slope eddy with an anticyclonal motion sitting just east of the shelf break front directly offshore of the STRATAFORM test area (Fig. 23). These warm eddies are known to have considerable influence on cross-frontal water mass movements and enhancements of chlorophyll in the shelf region.[43–45] This feature had a fairly important and variable influence on the waters over the shelf up to the 85-m bathymetric contour during the experiments.

Figures 24–26 show representative sound speed profiles measured at sites 1–3, respectively. At site 1, Fig. 24 shows the effect of the near surface warming, a mixed layer less than 10 m thick, a fairly equal thermocline and salinity front, with the cold pool of shelf water on the order of 10 to 20 m thick centered on 40-m water depth. The deeper water profiles show a strong influence of the shelf slope front, while the probes from 70 m and shallower show no influence at all from the slope waters, with the cold pool extending to the bottom.

At site 2, Fig. 25, three of the sound speed profiles show the presence of entrained gulf stream waters in the mid water column. These three profiles were the furthest east collected during the experiment. The warm waters from the gulf stream filament produced a high-speed sound layer in the water column for some areas deeper than the 80-m bathymetric contour. Outside the region of influence of this filament, however, there was the more normal behavior of the cold pool extending to the bottom west of the 70-m contour and the influence of the shelf break front deeper than 50 to 60 m in the water column. The thermocline moved up or down by ±5 m, while the lower to mid part of the water column was influenced by various filaments of warm water, creating a less stable sound speed profile than at site 1.

Site 3 was further towards the shelf edge, and measurements were sampled deeper than at the other two sites. In Fig. 26, the thermocline moved up and down on the order of ±5 m. There were cooler waters near the bottom for profiles taken shoreward of the mooring site, and a dominant presence of slope water in the near-bottom profiles further offshore. In these profiles slope waters themselves appear deeper than 95 m in the water column. This causes a fairly sharp upward refracting profile below the sound channel

axis. This caused less bottom interaction at site 3. Finally, in several profiles we observe the influence of fingers or filaments of warmer waters in the mid-water column.

The oceanographic measurements at the East Coast STRATAFORM show the interaction between the various water masses that influence the outer shelf water properties. This highlights the need for making high resolution temperature measurements, especially for understanding their effects on acoustic propagation in this region.

[1] N. C. Makris, Editor ''Geological Clutter Acoustics Experiment,'' Office of Naval Research Initial Report, Geoclutter Program, 27 April–5 May 2001.

[2] N. C. Makris and P. Ratilal, ''A unified model for reverberation and submerged object scattering in a stratified ocean waveguide,'' J. Acoust. Soc. Am. **109**, 909–941 (2001).

[3] P. Ratilal, N. C. Makris, and Y. Lai, ''Validity of the sonar equation and Babinet's principle for scattering in a stratified medium,'' J. Acoust. Soc. Am. **112**, 1797–1816 (2002).

[4] F. Ingenito, ''Scattering from an object in a stratified medium,'' J. Acoust. Soc. Am. **82**, 2051–2059 (1987).

[5] N. C. Makris, ''A spectral approach to 3-D object scattering in layered media applied to scattering from submerged spheres,'' J. Acoust. Soc. Am. **104**, 2105–2113 (1998).

[6] N. C. Makris, F. Ingenito, and W. A. Kuperman, ''Detection of a submerged object insonified by surface noise in an ocean waveguide,'' J. Acoust. Soc. Am. **96**, 1703–1724 (1994).

[7] F. B. Jensen, W. A. Kuperman, M. B. Porter, and H. Schmidt, *Computational Ocean Acoustics* (American Institute of Physics, New York, 1994).

[8] N. C. Makris, L. Z. Avelino, and R. Menis, ''Deterministic reveberation from ocean ridges,'' J. Acoust. Soc. Am. **97**, 3547–3574 (1995).

[9] N. C. Makris and C. S. Chia, ''The bi-azimuthal scattering distribution of an abyssal hill,'' J. Acoust. Soc. Am. **106**, 2491–2512 (1999).

[10] C. S. Chia, N. C. Makris, and L. T. Fialkowski, ''A comparison of bistatic scattering from two geologically distinct abyssal hills,'' J. Acoust. Soc. Am. **108**, 2053–2070 (2000).

[11] J. R. Preston and T. Akal, ''Analysis of backscattering data in the Tyrrhenian Sea,'' J. Acoust. Soc. Am. **87**, 119–134 (1990).

[12] M. D. Max, N. Portunato, and G. Murdoch, ''Sub-seafloor buried reflectors imaged by low frequency active sonar,'' SACLANTCEN memorandum, SM-306, SACLANT Centre, La Spezia, Italy (1996).

[13] C. A. Nittrouer, ''STRATAFORM: overview of its design and synthesis of its results,'' Mar. Geol. **154**(1–4), 3–12 (1999).

[14] C. S. Duncan, J. A. Goff, J. A. Austin, and C. S. Fulthorpe, ''Tracking the last sea-level cycle: seafloor morphology and shallow stratigraphy of the latest Quaternary New Jersey middle continental shelf,'' Mar. Geol. **170**, 395–421 (2000).

[15] J. A. Goff, D. Swift, C. S. Duncan, L. A. Mayer, and J. Hughes-Clarke, ''High-resolution swath sonar investigation of sand ridge, dune and ribbon morphology in the offshore environment of the New Jersey margin,'' Mar. Geol. **161**, 307–337 (1999).

[16] C. S. Duncan and J. A. Goff, ''Relict iceberg keel marks on the New Jersey outer shelf, southern Hudson apron,'' Geology **29**, 411–414 (2001).

[17] R. B. Evans and W. M. Carey, ''Reproducibility of low-frequency shallow-water acoustic experimental data,'' J. Acoust. Soc. Am. **99**, 2523–2529 (1996).

[18] K. M. Becker, G. V. Frisk, and S. D. Rajan, ''Geoacoustic inversion results from the modal mapping experiment,'' J. Acoust. Soc. Am. **107**, 2775 (2000).

[19] A. Turgut and S. Wolf, ''Matched-field inversion of seabed geoacoustic properties complemented by chirp sonar surveys,'' J. Acoust. Soc. Am. **110**, 2661 (2001).

[20] C. I. Malme, P. Jameson, P. McElroy, D. Stracher, G. Thomas, and D. Zwillinger, ''Development of a High Target Strength Passive Acoustic Reflector for Low Frequency Sonar Applications,'' BBN Report No. 7943. BBN Technologies, New London, CT.

[21] N. C. Makris and J. M. Berkson, ''Long-range backscatter from the Mid-Atlantic Ridge,'' J. Acoust. Soc. Am. **95**, 1865–1881 (1994).

[22] N. C. Makris, ''Imaging ocean-basin reverberation via inversion,'' J. Acoust. Soc. Am. **94**, 983–993 (1993).

[23] G. Bar-Yehoshua, ''Quantifying the effect of dispersion in continental shelf sound propagation,'' Master's thesis, MIT, 2002.

[24] J. W. Goodman, *Statistical Optics* (Wiley, New York, 1985).

[25] N. C. Makris, "The effect of saturated transmission scintillation on ocean acoustic intensity measurements," J. Acoust. Soc. Am. **100**, 769–783 (1996).

[26] J. Austin, J. Goff, S. Gulick, C. Fulthorpe, S. Nordfjord, M. Wiederspahn, S. Saustrup, S. Schock, J. Wulf, K. Gjerding, L. Mayer, and C. Sommerfield, "Assessing the "Geo," in GEOCLUTTER: New chirp sonar, sampling, and compressional wave velocity results from the New Jersey shelf," Eos. Trans. AGU. **82**(47), Fall Meet. Suppl. Abstract OS42A-0456 (2001).

[27] C. S. Fulthorpe, J. A. Goff, J. A. Austin, S. P. Gulick, and S. Nordfjord, "Late Quaternary Incisions and Related Shallow Subsurface Stratigraphy on the New Jersey Mid-Outer Shelf: Preliminary Results from Ultra-High Resolution Chirp Sonar Images—Part II," EOS Trans. AGU, **83**, Fall Meet. Suppl., Abstract OS71C-0300 (2001).

[28] J. A. Goff and S. Nordfjord, "Interpolation of fluvial morphology using channel-oriented coordinate transformation: A case study from the New Jersey shelf," submitted to Mathematical Geology.

[29] N. C. Makris, P. Ratilal, Y. Lai, and E. K. Scheer, "The Geoclutter experiment: Remotely imaging sub-bottom geomorphology in shallow water," J. Acoust. Soc. Am. **110**, 2742 (2001).

[30] R. C. Gauss, R. W. Nero, and D. Wurmser, "A Lloyd-mirror model to estimate the scattering strength of fish near rough ocean boundaries," J. Acoust. Soc. Am. **104**, 1820(A) (1998).

[31] R. Gauss, R. F. Gragg, R. W. Nero, D. Wurmser, and J. M. Fialkowski, "Broadband models for predicting bistatic bottom, surface, and volume scattering strengths," NRL Report, NRL/FR/7100-02-10,042 (2002).

[32] P. Ratilal, "Remote sensing of submerged objects and geomorphology in continental shelf waters with acoustic waveguide scattering," Ph.D Thesis, MIT, 2002.

[33] P. Ratilal and N. C. Makris, "Coherent versus diffuse surface and volume reverberation in an ocean wave guide: Reverberation rings, modal decoupling, and possible fish scattering in Geoclutter 2001," J. Acoust. Soc. Am. **112**, 2280 (2002).

[34] R. W. Nero, "Fish scattering during Boundary Characterization 2001," in *Proceedings of Geoclutter and Boundary Characterization 2001: Acoustic Interaction with the Seabed*, Halifax, October 2001, edited by P. C. Hines, N. C. Makris, and C. W. Holland, published by the Defence Research Establishment Atlantic, DREA TM-2001-185 (2001), pp. 39–42.

[35] R. W. Nero, C. H. Thompson, and R. H. Love, "Fish schools as potential clutter and false targets: Observations on the New Jersey shelf," J. Acoust. Soc. Am. **112**, 2280–2281 (2002).

[36] D. E. Weston and J. Revie, "A 5-day long-range sonar record of an extensive concentration of fish," J. Acoust. Soc. Am. **86**, 1608–1611 (1989).

[37] C. Holland, "Self-Consistent Measurements of Seabed Reflection and Scattering in the STRATAFORM Area," in *Proceedings of Geoclutter and Boundary Characterization 2001: Acoustic Interaction with the Seabed*, Halifax, October 2001, edited by P. C. Hines, N. C. Makris, and C. W. Holland, published by the Defence Research Establishment Atlantic, DREA TM-2001-185 (2001), pp. 12–20.

[38] G. Gawarkiewicz, T. G. Ferdelman, T. M. Church, and G. W. Luther III, "Shelf break frontal structure on the continental shelf north of Cape Hatteras," Cont. Shelf Res. **16**, 1751–1773 (1996).

[39] R. W. Houghton, F. Aikman III, and H. W. Ou, "Shelf-slope frontal structure and cross-shelf exchange at the New England shelf break," Cont. Shelf Res. **8**, 687–710 (1988).

[40] C. A. Linder and G. Gawarkiewicz, "A climatology of the shelfbreak front in the Middle Atlantic Bight," J. Geophys. Res. **103**, 18405–18424 (1998).

[41] R. W. Houghton, R. Schlitz, R. C. Beardsley, B. Bufman, and J. L. Chamberlain, "The Middle Atlantic Bight cold pool: evolution of the temperature structure during summer 1979," J. Phys. Oceanogr. **12**, 1019–1029 (1982).

[42] A. Ruffa, J. Bard, and M. Sundvik, "Demonstration test of LBVDS instrumented tow cable in waters South of New England—Initial Results," in Oceans 2000 Conference Proceedings, Providence, RI, October 2000.

[43] J. A. Barth, D. Bogucki, S. D. Pierce, and P. M. Kosro, "Secondary circulation associated with a shelfbreak front," Geophys. Res. Lett. **25**, 2761–2764 (1998).

[44] G. Gawarkiewicz, F. Bahr, R. C. Beardsley, and K. H. Brink, "Interaction of a slope eddy with the shelfbreak front in the Middle Atlantic Bight," J. Phys. Oceanogr. **31**, 2783–2796 (2001).

[45] J. P. Ryan, J. A. Yoder, and D. W. Townsend, "Influence of a Gulf Stream warm-core ring on water mass and chlorophyll distributions along the southern flank of Georges Bank," Deep-Sea Res., Part II **48**, 159–178 (2000).